

On the Configuration and Initialization of a Large Scale Hydrological Land Surface Model to Represent Permafrost

1 Mohamed E. Elshamy^{1*}, Daniel Princz², Gonzalo Sapriza-Azuri³, Mohamed S. Abdelhamed¹, Al Pietroniro¹,
2 Howard S. Wheater¹, and Saman Razavi¹

3 ¹ Global Institute for Water Security, University of Saskatchewan, 11 Innovation Blvd, Saskatoon, SK,
4 Canada S7N 3H5

5 ² Environment and Climate Change Canada, 11 Innovation Blvd, Saskatoon, SK, Canada S7N 3H5

6 ³ Departamento del Agua, Centro Universitario Regional Litoral Norte, Universidad de la República, Salto,
7 Uruguay

8 ***Corresponding author:** mohamed.elshamy@usask.ca

Abstract

9 Permafrost is an important feature of cold region hydrology, particularly in river basins such as the
10 Mackenzie River Basin (MRB), and needs to be properly represented in hydrological and land surface
11 models (H-LSMs) built into existing Earth System models (ESMs), especially under the unprecedented
12 climate warming trends that have been observed. Higher rates of warming have been reported in high
13 latitudes compared to the global average, resulting in permafrost thaw with wide-ranging implications for
14 hydrology and feedbacks to climate. The current generation of H-LSMs is being improved to simulate
15 permafrost dynamics by allowing deep soil profiles and incorporating organic soils explicitly. Deeper soil
16 profiles have larger hydraulic and thermal memories that require more effort to initialize. This study aims
17 to devise a robust, yet computationally efficient, initialization and parameterization approach applicable
18 to regions where data are scarce and simulations typically require large computational resources. The
19 study further demonstrates an upscaling approach to inform large-scale ESM simulations based on the
20 insights gained by modelling at small scales. We used permafrost observations from three sites along the
21 Mackenzie River Valley spanning different permafrost classes to test the validity of the approach. Results
22 show generally good performance in reproducing present-climate permafrost properties at the three
23 sites. The results also emphasize the sensitivity of the simulations to the soil layering scheme used, the
24 depth to bedrock and the organic soil properties.

Keywords

25 Hydrological Land Surface Models, Permafrost, Initialization, Organic Soils, Mackenzie River Basin

1. Introduction

26 Earth system models (ESMs) are widely used to project climate change and they show a current global
27 warming trend that is expected to continue during the 21st century and beyond (IPCC, 2014). Higher rates
28 of warming have been observed in high latitudes compared to the global average (DeBeer et al., 2016;
29 McBean et al., 2005) resulting in permafrost thaw with implications for soil moisture, hydraulic
30 connectivity, streamflow seasonality, land subsidence, and vegetation (Walvoord and Kurylyk, 2016).
31 Recent analyses provided by Environment and Climate Change Canada (Zhang et al., 2019) have shown
32 that Canada's far north has already seen an increase in temperature of double the global average, with
33 some portion of the Mackenzie River Basin already heating up by 4°C between 1948 and 2016. Subsequent
34 impacts on water resources in the region however, are not so clear. Recent analysis of trends in Arctic
35 freshwater inputs (Durocher et al., 2019) highlights that Eurasian rivers show a significant annual
36 discharge increase during 1975-2015 period while in North America, only rivers flowing into the Hudson
37 Bay region in Canada show a significant annual discharge change during that same period. Those rivers in
38 Canada flowing directly into the Arctic, of which the Mackenzie River provides the majority of flow, show
39 very little change at the annual scale. However, while the annual scale change may be small, larger
40 changes have been reported at the seasonal scale for Northern Canada (St. Jacques and Sauchyn, 2009;
41 Walvoord and Striegl, 2007) and Northeastern China (Duan et al., 2017). In the most recent assessment
42 of climate change impacts on Canada, Bonsal et al. (2019) reported that higher winter flows, earlier spring
43 flows, and lower summer flows were observed for some Canadian rivers. However, they also state that
44 "It is uncertain how projected higher temperatures and reductions in snow cover will combine to affect
45 the frequency and magnitude of future snowmelt-related flooding".

46 As permafrost underlies about one quarter of the exposed land in the Northern hemisphere (Zhang et al.,
47 2008), it is imperative to study and accurately model its behaviour under current and future climate
48 conditions. Knowledge of permafrost conditions (temperature, active layer thickness - ALT, and ground
49 ice conditions) and their spatial and temporal variations is critical for planning of development in Northern
50 Canada (Smith et al., 2007) and other Arctic environments. The hydrological response of cold regions to
51 climate change is highly uncertain, due to a large extent to our limited understanding and representation
52 of how the different hydrologic and thermal processes interact, especially under changing climate
53 conditions. Despite advances in cold-region process understanding and modelling at the local scale (e.g.
54 Pomeroy et al., 2007), their upscaling and systematic evaluation over large domains remain rather elusive.
55 This is largely due to lack of observational data, the local nature of these phenomena and the complexity

56 of cold-region systems. Hydrological response and land-surface feedbacks in cold-regions are generally
57 complex and depend on a multitude of inter-related factors including changes to precipitation intensity,
58 timing, and phase as well as soil composition and hydraulic and thermal properties.

59 There have been extensive regional and global modelling efforts focusing on permafrost (refer to
60 Riseborough et al., 2008; Walvoord and Kurylyk, 2016 for a review), using thermal models (e.g. Wright et
61 al., 2003), global hydrological models coupled to energy balance models (e.g. Zhang et al., 2012) and, most
62 notably, land surface models (e.g. Lawrence and Slater, 2005). These studies, however, have typically
63 focused on and modeled only a shallow soil column in the order of a few meters. For example, the
64 Canadian Land Surface Scheme (CLASS) typically uses 4.1m (Verseghy, 2012) and the Joint UK Land
65 Environment Simulator (JULES) standard configuration is only 3.0m (Best et al., 2011). These are too
66 shallow to represent permafrost properly and could result in misleading projections. For example,
67 Lawrence and Slater (2005) used a 3.43m soil column to project the impacts of climate change on near-
68 surface permafrost degradation in the Northern hemisphere using the Community Climate System Model
69 (CCSM3), which lead to overestimation of climate change impacts and raised considerable criticism (e.g.
70 Burn and Nelson, 2006). It eventually lead to further development of the Community Land Model (CLM),
71 the land surface scheme of the CCSM, to include deeper soil profiles (e.g. Swenson et al., 2012). Similarly,
72 the first version of CHANGE land surface model had only an 11m soil column (Park et al., 2011), which was
73 increased to 30.5m in subsequent versions (Park et al., 2013). Recognizing this issue, most recent studies
74 have indicated the need to have a deeper soil column (20-25m at least) in land surface models (run stand-
75 alone or embedded within ESMs) than previously used, to properly capture changes in freeze and thaw
76 cycles and active layer dynamics (Lawrence et al., 2012; Romanovsky and Osterkamp, 1995; Saprizia-Azuri
77 et al., 2018).

78 However, a deeper soil column implies larger soil hydraulic and, more importantly, thermal memory that
79 requires proper initialization to be able to capture the evolution of past, current and future changes. Initial
80 conditions are established by either spinning up the model for many annual cycles (or multi-year historical
81 cycles, sometimes de-trended) to reach some steady state or by running it for a long transient simulation
82 for 100s of years or both (spinning to stabilization followed by a long transient simulation). Lawrence et
83 al. (2008) spun up CLM v3.5 for 400 cycles with year 1900 data for deep soil profiles (50-125m) to assess
84 the sensitivity of model projections to soil column depth and organic soil representation. Dankers et al.
85 (2011) used up 320 cycles of the first year of record to initialize JULES to simulate permafrost in the Arctic.
86 Park et al. (2013) used 21 cycles of the first 20 years of their climate record (1948-2006) to initialize their

87 CHANGE land surface model to study differences in active layer thickness between Eurasian and North
88 American watersheds.

89 Conversely, Ednie et al. (2008) inferred from borehole observations in the Mackenzie Valley that present
90 day permafrost is in disequilibrium with current climate, and therefore, it is unlikely that we can establish
91 a reasonable representation of current ground thermal conditions by employing present or 20th century
92 climate conditions to start the simulations. Analysis of paleo-climatic records (Szeicz and MacDonald,
93 1995) of summer temperature at Fort Simpson, dating back to the early 1700s, shows that a negative
94 (cooling) trend prevailed until the mid-1800s followed by a positive (warming) trend until present.
95 However the authors “assumed” a quasi-equilibrium period prior to 1720, using an equilibrium thermal
96 model to establish the initial conditions of 1721 and then the temperature trends thereafter to carry out
97 a transient simulation until 2000. Thermal models use air temperature as their main input while land
98 surface models (as used here and described below) consider a suite of meteorological inputs and consider
99 the interaction between heat and moisture. The effect of soil moisture, and ice in particular, could be
100 large on the thermal properties of the soil. Sapriz-Azuri et al. (2018) used tree-ring data from Szeicz and
101 Macdonald (1995) to construct climate records for all variables required by CLASS at Norman Wells in the
102 Mackenzie Valley since 1638 to initialize the soil profile of their model. While useful, such proxy records
103 are not easily available at most sites. Additionally, re-constructing several climatic variables from summer
104 temperature introduces significant uncertainties that need to be assessed. Thus, there is a need to
105 formulate a more generic way to define the initial conditions of soil profiles for large domains.

106 Concerns for appropriate subsurface representation not only include the profile depth. The vertical
107 discretization of the soil column (the number of layers and their thicknesses) requires due attention. Land
108 surface models that utilize deep soil profiles exponentially increase the layer thicknesses to reach the total
109 depth using a tractable number of layers (15-20). For example, CLM 4.5 (Oleson et al., 2013) used 15 layers
110 to reach a depth of 42.1m for the soil column. Sapriz-Azuri et al. (2018) used 20 layers to reach a depth
111 of 71.6m in their experiments using MESH/CLASS. Park et al. (2013) had a 15-layer soil column with
112 exponentially increasing depth to reach a total depth of 30.5m in the CHANGE land surface model. Clearly,
113 the role of the soil column discretization needs to be addressed.

114 The importance of insulation from the snow cover on the ground and/or organic matter in the upper soil
115 layers is key to the quality of ALT simulations (Lawrence et al., 2008; Park et al., 2013). Organic soils have
116 large heat and moisture capacities that, depending on their depth and composition, moderate the effects
117 of the atmosphere on the deeper permafrost layers and work all year round but could lead to deeper frost

118 penetration in winter (Dobinski, 2011). Snow cover, in contrast, varies seasonally and inter-annually and
119 can thus induce large variations to the ALT, especially in the absence of organic matter (Park et al., 2011).
120 Climate change impacts on precipitation intensity, timing, and phase are translated to permafrost impacts
121 via the changing the snow cover period, spatial extent, and depth. Therefore, it is critical to the simulation
122 of permafrost that the model includes organic soils and has adequate representation of snow
123 accumulation (including sublimation and transport) and melt processes.

124 This study proposes a generic approach to initialize deep soil columns in land surface models and
125 investigates the impact of the soil column discretization and the configurations of organic soil layers (how
126 many and which type) on the simulation of permafrost characteristics. This is done through detailed
127 studies conducted at three sites in the Mackenzie River valley, located in different permafrost zones. The
128 objective is to be able to generalize the findings to the whole Mackenzie River Basin and elsewhere, rather
129 than finding the best configuration for the selected sites. Using the same modelling framework at both
130 small and large scales is key to facilitating such generalization.

2. Models, Methods, and Datasets

2.1 The MESH Modelling Framework

131 MESH is a community hydrological land surface model (H-LSM) coupled with two-dimensional
132 hydrological routing (Pietroniro et al., 2007). It has been widely used in Canada to study the Great Lakes
133 Basin (Haghnegahdar et al., 2015) and the Saskatchewan River Basin (Yassin et al., 2017, 2019a) amongst
134 others. Several applications to basins outside Canada are underway (e.g. Arboleda-Obando, 2018;
135 Bahremand et al., 2018). The MESH framework allows coupling of a land surface model, either CLASS
136 (Verseghy, 2012) or SVS (Husain et al., 2016) that simulates the vertical processes of heat and moisture
137 flux transfers between the land surface and the atmosphere, with a horizontal routing component
138 (WATROUTE) taken from the distributed hydrological model WATFLOOD (Kouwen, 1988). Unlike many
139 land surface models, the vertical column in MESH has a slope that allows for lateral transfer of overland
140 flow and interflow (Soulis et al., 2000) to an assumed stream within each grid cell of the model. MESH
141 uses a regular latitude-longitude grid and represents subgrid heterogeneity using the grouped response
142 unit (GRU) approach (Kouwen et al., 1993) which makes it semi-distributed. In the GRU approach,
143 different land covers within a grid cell do not have a specific location and common land covers in adjacent
144 cells share a set of parameters, which simplifies basin characterization. While land cover classes are
145 typically used to define a GRU, other factors can be included in the definition such as soil type, slope,

146 aspect. MESH has been under continuous development; its new features include improved representation
147 of baseflow (Luo et al., 2012), controlled reservoirs (Yassin et al., 2019b) as well as permafrost (this paper).
148 For this study, we use CLASS as the underlying land surface model within MESH.

149 Underground, CLASS couples the moisture and energy balances for a user-specified number of soil layers
150 of user-specified thicknesses, which are uniform across the domain. Each soil layer, thus, has a diagnosed
151 temperature and both liquid and frozen moisture contents down to the soil permeable depth or the
152 “depth to bedrock – SDEPTH” below which there is no moisture and the thermal properties of the soil are
153 assumed as those of bedrock material (sandstone). MESH usually runs at 30min time step and thus from
154 the MESH-simulated continuous temperature profiles, one can determine several permafrost related
155 aspects that are used in the presented analyses such as (see Figure 1):

156 - Temperature envelopes (Tmax and Tmin) at daily, monthly and annual time steps, defined by the
157 maximum and minimum simulated temperature for each layer over the specified time period. To
158 compare with available observations, we use the annual envelopes.

159 - Active layer thickness (ALT) defined as the maximum depth, measured from the ground surface,
160 of the zero isotherm over the year taken from the annual maximum temperature envelopes by
161 linear interpolation between layers bracketing the zero value (freezing point depression is not
162 considered) and has to be connected to the surface. The daily progression of the ALT can also be
163 generated to visualize the thaw and freeze fronts and determine the dates of thaw and freeze-
164 up. These are calculated in a similar way to the annual ALT but using daily envelopes.

165 - Depth of the zero annual amplitude (DZAA) where the annual temperature envelopes meet to
166 within 0.1° (van Everdingen, 2005) and the temperature at this depth (TZAA).

167

168 **Possible position for Figure 1**

169 Permafrost is usually defined as ground that remains cryotic (i.e. temperature $\leq 0^{\circ}\text{C}$) for at least two years
170 (Dobinski, 2011; van Everdingen, 2005) but for modelling purposes and to validate against annual ground
171 temperature envelopes and ALT observations, a one-year cycle is adopted. This is common amongst the
172 climate and land surface modelling community (e.g. Park et al., 2013). van Everdingen (2005) defined the
173 active layer thickness as the thickness of the layer that is subject to annual thawing and freezing in areas
174 underlain by permafrost. Strictly speaking, the active layer thickness should be the lesser of the maximum
175 seasonal frost depth and the maximum seasonal thaw depth (Walvoord and Kurylyk, 2016). The maximum
176 frost depth can be less than the maximum thaw depth and, in such a case there, is a layer above the

177 permafrost that is warmer than 0°C but is not connected to the surface (a lateral talik). Because active
178 layer observations are usually based on measuring the maximum thaw depth, we adopted the same (thaw
179 rather than freeze) criterion when calculating ALT in the model.

180 Prior versions of MESH/CLASS merely outputted temperature profiles. The code has been amended to
181 calculate the additional permafrost-related outputs detailed above. A typical CLASS configuration consists
182 of 3 soil layers of 0.1, 0.25, and 3.75m thickness but in 2006, the CLASS code was amended to
183 accommodate as many layers as needed (Verseghy, 2012). Neglecting lateral heat flow, the one
184 dimensional finite difference heat conservation equation is applied to each layer to obtain the change in
185 average layer temperature \bar{T}_i over a time step Δt as:

$$186 \quad \bar{T}_i^{t+1} = \bar{T}_i^t + [G_{i-1}^t - G_i^t] \frac{\Delta t}{C_i \Delta z_i} \pm S_i \quad (1)$$

187 where, t denotes the time, i is the layer index, and G_{i-1} and G_i are the downward heat flux at the top and
188 bottom of the soil layer, respectively, Δz_i is the thickness of the layer, C_i is the volumetric heat capacity
189 and S_i is a correction term applied when the water phase changes (freezing or thawing) or the water
190 percolates (exits the soil column at the lowest boundary). The volumetric heat capacity of the layer is
191 calculated as the sum of the heat capacities, C_j , of its constituents (liquid water, ice, soil minerals, and
192 organic matter), weighted by their volume fractions θ_j and, therefore, varies with time depending on the
193 moisture content:

$$194 \quad C_i = \sum_j C_j \theta_j \quad (2)$$

195 Heat fluxes between soil layers are calculated using the layer temperatures at each time step using the
196 one-dimensional heat conduction equation:

$$197 \quad G(z) = -\lambda(z) \frac{dT}{dz} \quad (3)$$

198 where $\lambda(z)$ is the thermal conductivity of the soil calculated analogously to the heat capacity. Temperature
199 variation within each soil layer is assumed to follow a quadratic function of depth (z). Setting the flux at
200 the bottom boundary to a constant (i.e. Neumann type boundary condition for the differential equation)
201 and diagnosing the flux into the ground surface, $G(0)$, from the solution of the surface energy balance,
202 results in a linear equation for $G(0)$ as a function of \bar{T}_i for the different layers in addition to soil surface
203 temperature, $T(0)$. This enables diagnosing the fluxes and temperatures of all layers using a forward
204 explicit scheme. More details are given in Section S1 of the supplementary material and full details are
205 given in Verseghy (2012, 1991).

206 The CLASS thermal boundary condition at the bottom of the soil column is either no-flux (i.e. the gradient
207 of the temperature profile should be zero) or a constant geothermal flux. For this study, we considered
208 the no-flux condition, as data for the geothermal flux are not easy to find at the MRB scale. Nicolsky et al.
209 (2007) ignored the geothermal flux in their study over Alaska using CLM with an 80m soil column. Sapriza-
210 Azuri et al. (2018) showed that the difference in temperature at DZAA between the two cases is within
211 the error margin for geothermal temperature measurements for 60% of their simulations at Norman
212 Wells. However, we also tested with a constant geothermal flux to verify those previous findings.

213 As for organic soils, CLASS can use a percentage of organic matter within a mineral soil layer, a fully organic
214 layer, or thermal and hydraulic properties provided directly. As the latter are not usually available,
215 especially at large scales, we used the first two options. In the first case, the organic content is used to
216 modify soil hydraulic and thermal properties, similar to CLM (Oleson et al., 2013). For fully organic soils,
217 CLASS has special values for those properties depending on the type of organic soil selected (fibril, hemic
218 or sapric) based on the work of Letts et al. (2000) for peat soils (see Section S1). In traditional CLASS
219 applications, when the organic soil flag is activated, fibril (type 1) parameters are assigned to the first soil
220 layer, hemic (type 2) parameters to the second, and sapric (type 3) parameters to deeper layers as soon
221 (Verseghy, 2012) – see Supplement Table S1 for parameter values. The corresponding code in MESH was
222 amended such that more than one fibril or hemic layer can be present, and that the organic soil flag can
223 be switched off (returning to a mineral soil parameterization) for lower layers. In assigning the organic
224 layer type, the same order is used (fibril at the surface, followed by hemic, then sapric with depth), as this
225 represents the natural decomposition process, but with the introduction of many more layers with depth,
226 it is necessary to have more flexibility in how the organic layers can be configured. The fully organic
227 parameterization was activated when the organic content is 30% or more, based on recommendation by
228 the Soil Classification Working Group (1998).

2.2 Study Sites and Permafrost Data

229 The Mackenzie River Basin (MRB) extends between 102-140°W and 52-69°N (Figure 2). It drains an area
230 of about 1.775 Mkm² of Western and Northwestern Canada and covers parts of the provinces of
231 Saskatchewan, Alberta and British Columbia, as well as the Yukon and the Northwest Territories. The
232 average annual discharge at the basin outlet to the Beaufort Sea exceeds 300 km³, which is the fifth largest
233 discharge to the Arctic. Such a large discharge influences regional as well as global circulation patterns
234 under the current climate, and is expected to have implications for climate change. Figure 2 also shows
235 the permafrost extent and categories for the MRB taken from the Canadian Permafrost Map

236 (Hegginbottom et al., 1995). About 75% of the basin is underlain by permafrost that can be either
237 continuous (in the far North and the Western Mountains), discontinuous (to the south of the continuous
238 region), sporadic (in the southern parts of the Liard and in the Hay sub-basin), or patchy further south. It
239 is important to properly represent permafrost for the MRB model, given the current trends of thawing
240 and its major impacts on landforms, connectivity, and thus the hydrology of the basin. This is achieved
241 through detailed studies conducted at three sites along a transect near the Mackenzie River going from
242 the Sporadic permafrost zone (Jean Marie River) to the Extensive Discontinuous zone (Norman Wells) and
243 the Extensive Continuous zone (Havikpak Creek) as shown in Figure 3. The following paragraphs give brief
244 descriptions of the three sites. Table 1 gives details of permafrost monitoring at the sites while more
245 detailed descriptions are given in Section S2 of the supplementary material.

246 **Possible position for Figure 2**

247 **Possible position for Table 1**

248 The Jean Marie River (JMR) is a tributary of the main Mackenzie River Basin (Figure 3a) in the Northwest
249 Territories (NWT) of Canada. The basin is dominated by boreal (deciduous, coniferous and mixed) forest
250 on raised peat plateaux and bogs. The basin is located in the sporadic permafrost zone where permafrost
251 underlies few spots only and is characterized by warm temperatures ($> -1^{\circ}\text{C}$) and limited ($< 10\text{m}$) thickness
252 (Smith and Burgess, 2002). The basin and adjacent basins (e.g. Scotty Creek) have been subject to
253 extensive studies because the warm, thin, and sporadic permafrost underling the region has been rapidly
254 degrading (Calmels et al., 2015; Quinton et al., 2011). Several permafrost-monitoring sites have been
255 established in and around the basin mostly as part of the Norman Wells to Zama pipeline monitoring
256 program launched by the Government of Canada and Enbridge Pipeline Inc. in 1984-1985 (Smith et al.,
257 2004) to investigate the pipeline impact on permafrost conditions. This study uses data from sites 85-12A
258 and 85-12B (see Table 1). Site 85-12A has no permafrost while site 85-12B, in close proximity, has a thin
259 (3-4m) permafrost layer with an ALT of about 1.5m as estimated from soil temperature envelopes over
260 the period 1986-2000. See Figure S1 in the supplementary material for a plot of observed temperature
261 envelopes.

262 **Possible position for Figure 3**

263 Bosworth Creek (BWC) has a small basin draining from the northeast to the main Mackenzie River near
264 Norman Wells (Figure 3b). Permafrost monitoring activities started in the region in 1984 with the
265 construction of the Norman Wells-Zama buried oil pipeline (as described above). The basin is dominated

266 by boreal (deciduous, coniferous and mixed) forest. It is located in the extensive discontinuous permafrost
267 zone with relatively deep active layer (1-3 m) and relatively thick (10-50m) permafrost (Smith and Burgess,
268 2002). Saprizia-Azuri et al. (2018) used cable T5 at the pump station site (84-1) to investigate the
269 appropriate soil depth and initial conditions for their permafrost simulations, which serve as a pre-cursor
270 for this current study. They recommended a soil depth of at least 20m to ensure that the simulated DZAA
271 is within the soil profile. However, they based their analysis on cable T5, which is within the right of way
272 of the pipeline and is likely to be affected by its construction/operation. We focus on the Norman Wells
273 pump station site (84-1) and for this study we choose cable T4 as it is more likely to reflect the natural
274 permafrost conditions being out of the right of way of the pipeline. It has a continuous record since 1985
275 (Smith et al., 2004; Duchesne, personal communication, 2017).

276 Havikpak Creek (HPC) is a small arctic research basin (Figure 3c) located in the eastern part of the
277 Mackenzie River basin delta, 2km north of Inuvik Airport in the Northwest Territories (NWT). The basin is
278 dominated by sparse taiga forest and shrubs and is underlain by thick permafrost (>300m). The basin has
279 been subject to several hydrological studies, especially during the Mackenzie GEWEX Study (MAGS).
280 Recently, Krogh et al. (2017) modelled its hydrological and permafrost conditions using the Cold Regional
281 Hydrological Model (CRHM) (Pomeroy et al., 2007). They integrated a ground freeze/thaw algorithm
282 called XG (Changwei and Gough, 2013) within CRHM to simulate the active layer thickness and the
283 progression of the freeze/thaw front with time but they did not attempt to simulate the temperature
284 envelopes or DZAA. Ground temperatures are measured with temperature cables installed in boreholes
285 at two sites 01TC02 and 01TC03 respectively (Smith et al., 2016). In addition, there are three thaw tubes
286 at Inuvik Upper Air Station (90-TT-16) just to the west of the basin, at HPC proper (93-TT-02), and at the
287 Inuvik Airport bog site (01-TT-03) measuring the active layer depth and ground settlement (Smith et al.,
288 2009).

2.3 Land Cover Parameterization

289 Parameterizations for the three selected basins were extracted from a larger MRB model, described in
290 Elshamy et al. (in preparation). This includes the land cover characterization and parameters for
291 vegetation and hydrology. The land cover data are based on the CCRS 2005 dataset (Canada Centre for
292 Remote Sensing (CCRS) et al., 2010). The parameterization of certain land cover types differentiates
293 between the eastern and western sides of the basin using the Mackenzie River as a divide, informed by
294 calibrations of the MRB model. HPC and BWC are on the east side of the river while JMR is on the west
295 side and therefore these setups have different parameter values for certain GRU types (e.g. Needleleaf

296 Forest). SDEM, soil texture information and initial conditions were taken as described above and adjusted
297 according to model evaluation versus permafrost related observations (ALT, DZAA, temperature
298 envelopes) with the aim to develop an initialization and configuration strategy that can be implemented
299 for the larger MRB model.

300 Provisions for special land covers within the MESH framework include inland water.. Because of limitations
301 in the current model framework, inland water must be represented as a porous soil, which is
302 parameterized such that it remains as saturated as possible, drainage is prohibited from the bottom of
303 the soil column and it is modelled using CLASS with a large hydraulic conductivity value and no slope.
304 Additionally, it was initialized to have a positive bottom temperature and therefore, it does not develop
305 permafrost. Wetlands are treated in a similar way (impeded drainage and no slope) but with grassy
306 vegetation and preserving the soil parameterization as described in below in Sections 2.5 and 2.6. It
307 remains close to saturation but can still be underlain by permafrost, depending on location. Taliks are
308 allowed to develop under wetlands this way.

2.4 Climate Forcing

309 MESH requires seven climatic variables at a sub-daily time step to drive CLASS. For this study we used the
310 WFDEI dataset that covers the period 1979-2016 at 3 hourly resolution (Weedon et al., 2014). The dataset
311 was linearly interpolated from its original $0.5^\circ \times 0.5^\circ$ resolution to the MRB model grid resolution of 0.125°
312 $\times 0.125^\circ$. The high resolution forecasts of the Global Environmental Multiscale atmospheric model – GEM
313 (Côté et al., 1998b, 1998a; Yeh et al., 2002), and the Canadian Precipitation Analysis – CaPA (Mahfouf et
314 al., 2007) datasets, often combined as (GEM-CaPA), provide the most accurate gridded climatic dataset
315 for Canada in general (Wong et al., 2017). Unfortunately, these datasets are not available prior to 2002
316 when most of the permafrost observations used for model evaluation are available. However, an analysis
317 by Wong et al. (2017) showed that precipitation estimates from the CaPA and WFDEI products are in
318 reasonable agreement with station observations. Alternative datasets such as WFD (Weedon et al., 2011)
319 and Princeton (Sheffield et al., 2006) go earlier in time (1901) but are not being updated (WFD stops 2001
320 while Princeton stops 2012). Additionally, Wong et al. (2017) showed that the Princeton dataset has large
321 precipitation biases for many parts of Canada. Analysis of the sensitivity of the results presented here to
322 the choice of the climatic dataset is beyond the scope of this work.

2.5 Soil Profile and Permeable Depth

323 As mentioned earlier, Sapriza-Azuri et al. (2018) recommended a total soil column depth (D) of no less
324 than 20m to enable reliable simulation of permafrost dynamics considering the uncertainties involved
325 mainly due to parameters. Their study is relevant because they used the same model used in this study
326 (MESH/CLASS). They studied several profiles, down to 71.6m depth. Recent applications of other H-LSMs
327 also considered deep soil column depths; e.g. CLM 4.5 used 42.1m (Oleson et al., 2013) and CHANGE (Park
328 et al., 2013) used 30.5m. After a few test trials with D = 20, 25, 30, 40, 50 and 100m at the study sites, we
329 found that the additional computation time when adding more layers to increase D is outweighed by the
330 reliability of the simulations. The reliability criterion used here is that the temperature envelopes meet
331 (i.e. DZAA) well within the soil column depth over the simulation period (including spinning-up) such that
332 the bottom boundary condition does not disturb the simulated temperature profiles/envelopes and ALT
333 (Nicolksy et al., 2007). DZAA is a relatively stable indicator for this criterion (Alexeev et al., 2007). The
334 simulated DZAA reached a maximum of 20m at one of the sites in a few years and thus a total depth of
335 50m was used in anticipation for possible changes in DZAA with future warming. We show that this depth
336 is adequate at the three sites selected in the subsequent sections.

337 As noted above, the total soil column depth is only one factor in the configuration of the soil. The layering
338 is as critical. In former modelling studies, exponentially increasing soil layer thicknesses were used, aiming
339 to reach the required depth with a minimum number of layers. The exponential formulation creates more
340 layers near the surface, which allows the models to capture the strong soil moisture and temperature
341 gradients there and yet have a reasonable number of layers (15-20) to reduce the computational burden.
342 However, for most of the MRB, the observed ALT is in the range of 1-2m from the surface and the
343 exponential formulations increase layer thickness quickly after the first 0.5-1.0m, which reduces the
344 accuracy of the model, especially for transient simulations. Therefore, we adopted two layering schemes
345 that have more layers in the top 2m, and increased layer thicknesses at lower depths, to a total depth
346 near 50m. The first scheme has the first meter divided into 10 layers, the second meter divided into 5
347 layers and the total soil column has 23 layers. The second scheme has soil thicknesses increasing more
348 gradually to reach 51.24m in 25 layers following a scaled power law. This latter scheme has an advantage
349 that each layer is always thicker than the one above it (except the second layer), as the explicit forward
350 difference numerical scheme to solve the energy and water balances in CLASS can have instabilities when
351 layers in succession have the same thickness. The minimum soil layer thickness is taken as 10cm as advised

352 by Verseghy (2012). Table 2 shows the soil layer thicknesses and centers (used for plotting temperature
353 profiles/envelopes) for both soil layering schemes.

354 **Possible position of Table 2**

355 As mentioned before, the permeable depth (SDEP) marks the hydrologically active horizon below which
356 the soil is not permeable and where its thermal properties are changed to those of bedrock material. This
357 makes it an important parameter for not only for water storage but also for thermal conductance. It was
358 set for the various study basins from the Shangguan et al. (2017) dataset interpolated to 0.125°, the MRB
359 model grid resolution, by Keshav et al. (2019b). The sensitivity of the results to SDEP is assessed by
360 perturbing it within a reasonable range at each site as shown in the results.

2.6 Organic Soil Configuration

361 Organic soils were mapped from the Soil Landscapes of Canada (SLC) v2.2 (Centre for Land and Biological
362 Resources Research, 1996) for the whole MRB (Figure 4) at 0.125° resolution by Keshav et al. (2019a).
363 However, this dataset does not provide information on the depth of the organic layers or their
364 configuration (i.e. the thicknesses of Fibric, Hemic and Sapric layers in peaty soils). Therefore, different
365 configurations have been tested at the study sites based on available local information (Table 3). We also
366 compared fully organic configurations (ORG) at the three sites with mineral configurations with organic
367 content (M-org) to investigate the appropriate configuration at each site, keeping in mind the need to
368 generalize it for larger basins.

369 **Possible Position for Figure 4**

370 For JMR, we tested configurations with about 0.3m organic soil (3 layers) to over 2m of organic soil, where
371 organic content from SLC v2.2 ranged between 48-59% (Figure 4). The soil texture immediately below
372 these layers was characterized as a mineral soil of uniform texture with 15% sand and 15% clay content,
373 with the remainder assigned as silt. 4-7m peat depths in the surrounding region have been identified in
374 reports (Quinton et al., 2011) and by borehole data at permafrost monitoring sites (Smith et al., 2004).
375 Therefore, layers at these depths until bedrock were characterized as mineral soils (as described above),
376 but with 50% organic content. These deeper layers, while having considerable organic content, do not use
377 the previously described parameterization for fully organic soils. This is an exception for this basin, which
378 could be generalized for the MRB in areas with high organic content (e.g. > 50%) like this region. These
379 configurations are summarized in Table 3. For the M-org configuration, we used a decreasing organic
380 content with depth.

381

Possible position of Table 3

382 For BWC, the organic map indicated that organic matter ranges between 27-34%. We tested
 383 configurations with 0.3 – 0.8m organic layers. A borehole log for 84-1-T4 site (Smith et al., 2004) shows a
 384 thin organic silty layer at the top (close to 0.2-0.3m). Sand and clay content below the organic layers are
 385 uniformly taken to be 24% and 24% respectively based again on SLC v2.2 with the remainder (52%)
 386 assumed silt. We tested ORG and M-org configurations as shown Table 3.

387 The organic content indicated by the gridded soil information at HPC is only 18%, which is lower than the
 388 30% threshold decided for fully organic soils. However, Quinton and Marsh (1999) used a 0.5m thick
 389 organic layer in their conceptual framework developed to characterise runoff generation in the nearby
 390 Siksik creek. Krogh et al. (2017) adopted the same depth for their modelling study of HPC. Therefore, we
 391 tested configurations with 0.3-0.8m fully organic layers as well as the M-org configuration with a uniform
 392 18% organic content. Below that, soil texture values are taken to be 24% sand and 32% clay from SLC v2.2.

2.7 Spinning up and Stabilization

393 We used the first hydrological year of the climate forcing (Oct 1979-Sep 1980) to spin up the model
 394 repeatedly for 2000 cycles while monitoring the temperature and moisture (water and ice contents)
 395 profiles at the end of each cycle for stabilization. We checked that the selected year was close to average
 396 in terms of temperature and precipitation compared to the WFDEI record (1979-2016) – Table 4. The start
 397 of the hydrological year was selected because it is easier to initialize CLASS when there is no snow cover
 398 or frozen soil moisture content. Stabilization is assessed visually using various plots as well as by
 399 computing the difference between each cycle and the previous one making sure the absolute difference
 400 does not exceed 0.1°C for temperature (which is the accuracy of measurement of the temperature
 401 sensors) and 0.01 m³/m³ for moisture components for all soil layers. The aim is to determine the minimum
 402 number of cycles that could inform the ongoing development of the MRB model, as it is computationally
 403 very expensive to spin up the whole MRB domain for 2000 cycles. We then assessed the impact of running
 404 the model for the period 1980-2016 after 50, 100, 200, 500, 1000, and 2000 spin-up cycles on the ALT,
 405 DZAA, and the temperature envelopes at the three sites for selected years depending on the available
 406 observations. We assessed the quality of the simulations visually as well as quantitatively by calculating
 407 the root mean squared error (RMSE) for ALT, DZAA, and the temperature profiles.

408

Possible position of Table 4

3. RESULTS

3.1 Establishing Initial Conditions

409 Figure 5 shows the temperature profiles at the end of spinning cycles for a selected GRU (Needleleaf – NL
410 Forest) for the three selected sites using the two suggested soil layering schemes (SC1 and SC2) and using
411 two different organic configuration (ORG vs M-org) for SC2. NL Forest is representative of the vegetation
412 at the selected thermal sites for the three studied basins (except HPC bog site). As expected, the profile
413 changes quickly for the first few cycles then tends to stabilize such that no significant change occurs after
414 100 cycles and less in most cases. Similar observations can be made for soil moisture (both water and ice
415 contents) from Figure 6. Changes in moisture content tend to diminish more quickly than those for
416 temperature, especially for ORG, and thus we will focus on temperature changes in the remaining results.
417 However, water and ice fractions play important roles in defining the thermal properties of the soil and
418 provide useful insights to understand certain behaviours in the simulations. Figure 7 shows the
419 temperature of each layer for the same cases versus the cycle number to visualize the patterns of change
420 over the cycles. Small oscillations are observed, indicating minor numerical instabilities in the model, but
421 these do not cause major differences for the simulations. In some cases, the temperature keeps drifting
422 for several hundred cycles before stabilizing (if stabilization occurs). We note a few important findings:

- 423 • The temperature of the bottom layer (TBOT) remains virtually unchanged from its initial value. This
424 triggered further testing using different initial values and the impacts on stabilization were similar, as
425 shown in the next sections. We also checked the model behaviour for shallower soil columns and
426 found that the bottom temperature did change with spinning up, within a range that decreased as
427 the total soil depth increased.
- 428 • The vertical discretization of the soil plays an important role in the evolution of temporal moisture
429 and temperature profiles. SC2 results in faster stabilization than SC1 with less drifting for all cases.
- 430 • The depth of organic layers, and their sub-type in fully organic soils, controls the shape of the moisture
431 content profiles and the ice/water content partitioning. This in turn influences the soil thermal
432 properties (drier soils are generally less conductive, icy soils are more conductive) and thus affects the
433 number of cycles needed to reach stable conditions. Deeper fully organic soils (JMR) require more
434 cycles to stabilize than mineral ones with organic content.

435 **Possible Position of Figure 5**

436 **Possible Position of Figure 6**

437 The temperature gradient northward is clear comparing the different sites as well as the impact of the
438 deeper organic layers at JMR on the slower stabilization of temperature and, to a lesser extent, moisture
439 content. This is related to the low thermal conductivity of organic matter as well as the low moisture
440 content below the organic layers as peat acts as a sponge absorbing water and heat and disallowing
441 downward propagation, especially in the absence of ice (i.e. in summer). Hemic and sapric peat soils have
442 relatively high minimum water contents as shown in Figure 6 (see also Table S1 in the Supplement). The
443 M-org configuration allows more moisture to seep below the organic layers and have some higher ice
444 content at some depth that depends on the thickness of the organic layers and the general site conditions.
445 For example, it forms below the thick organic layers for JMR but it formed at a deeper depth at BWC as
446 the organic thickness is smaller. HPC has a comparable organic depth to BWC but the layers with high ice
447 content formed at a shallower depth because the site is colder. At all three sites, and for both ORG and M-
448 org configurations, there is a change in the slope of the temperature profile at the depth corresponding
449 to the interface of the soil to bedrock, illustrating the importance of the SDEP parameter for permafrost
450 simulations. This is caused by the change in soil thermal properties above and below SDEP (respective of
451 the two different mediums above and below this interface) and the moisture contents therein; bedrock
452 is assumed to remain dry at all times while soil will always have a minimum liquid water content depending
453 on its type.

454 **Possible Position of Figure 7**

455 Given the above findings, the remainder of the results focus on SC2 only. Additionally, we considered
456 different values for the bottom temperature based on site location and extrapolation of observed
457 temperature profiles, because it cannot be established through spin-up and ground temperature
458 measurements rarely go deeper than 20m. There are established strong correlations between near
459 surface ground temperature and air temperature at the annual scale (e.g. Smith and Burgess, 2000) but
460 the near surface ground temperature is taken just a few centimeters below the surface. We spin up the
461 model at the three sites for 2000 cycles for a few cases and then use the initial conditions after a selected
462 number of cycles to run a simulation for the period of record (1979-2016) and assess the differences for
463 ALT, DZAA, and temperature profiles. The sensitivity of the results to SDEP, TBOT, and the organic soil
464 depth will then be assessed using 100 spin cycles only.

3.2 Impact of Spinning up

465 Figure 8, Figure 9 and Figure 10 show the simulated ALT, DZAA and temperature envelopes (selected
466 years) at the three study sites respectively using initial conditions after 50, 100, 200, 500, 1000, and 2000

467 spin-up cycles using SC2 and the stated configuration for SDEP, TBOT, and ORG/M-org. Most differences
468 across the spin-up range are negligible. What stands out are some large differences in ALT and DZAA at
469 JMR for some years (ORG configuration only) depending on the initial conditions (i.e. number of cycles)
470 used. The low thermal conductivity of the thick fully organic layers slows the stabilization process and thus
471 yields slightly different initial conditions depending on the number of cycles used. That does not happen
472 for the two other sites with thinner ORG layers or for M-org configurations. This further emphasized by
473 the RMSE values for ALT and DZAA shown in the legends of Figure 8 and Figure 9.

474 **Possible Position of Figure 8**

475 Assuming that more spin-up cycles would lead to diminished differences, and thus considering the results
476 initiated after 2000 cycles as a benchmark, one can accept an error of a few centimeters in simulated ALT
477 using a smaller number of spin-up cycles. For JMR, this error is about 10% on average, which is much
478 smaller than the error in simulating ALT at this site. Thus, there is a trade-off in computational time by
479 limiting the number of cycles required for a slight loss of accuracy at some sites, particularly those located
480 in the more challenging sporadic zone.

481 **Possible Position of Figure 9**

482 The figures also include relevant observations, and RMSE values, to assess the quality of simulations. The
483 simulated ALT at JMR are over-estimated (Figure 8) by the ORG configuration. The M-org configuration
484 does better for mean ALT at JMR but is much worse than ORG for BWC which overestimates ALT by about
485 8m. For BWC, the ALT simulation under ORG is close to observations for most years but the simulation
486 shows more inter-annual variability while observations show a small upward trend after an initial period
487 of large increase (1988-1992), which may be the result of the disturbance of establishing the site. A couple
488 of observations are marked “extrapolated” as the zero isotherm falls above the first thermistor (located
489 1m deep). For HPC, M-org better represents the conditions at 01TC02 while ORG resulting in a smaller
490 ALT on average and is closer to the thaw tube measurements at HPC (93-TT-02), as indicated by the RMSE
491 values. This is indicative of the large heterogeneity of conditions that can occur in close proximity to each
492 other and that require different modelling configurations. M-org configurations generally show little to
493 no inter-annual variability (except for HPC) while ORG ones show more inter-annual variability.

494 The simulated DZAA (Figure 9) is over-estimated at JMR under both ORG and M-org configurations while
495 it is close to values deduced from observations at BWC and HPC. In contrast to ALT, DZAA observations
496 have larger inter-annual variability than simulation, possibly due to the large spacing of measuring

497 thermistors and the failure of some in some years. For HPC, both ORG and M-org simulations are showing
498 more variability in DZAA than the depth deduced from observations for 01TC02 and both underestimate
499 it. In general, matching DZAA to observations is not an objective in itself but its occurrence well within the
500 selected soil depth is more important. The largest value simulated is about 19m for HPC, which is less than
501 half the total soil depth. This indicates that a smaller soil column depth would not be suitable for HPC but
502 could be used for JMR and BWC.

503 **Possible Position of Figure 10**

504 Comparing temperature profiles for a selected year at each site (Figure 10) reveals large difference
505 between ORG and M-org configurations, especially at HPC and BWC. The overall shapes of the profiles
506 depend on the selected configuration. M-org works better for HPC while ORG is better at BWC. Both
507 configurations do relatively well for JMR although this site is characterized with deep peat. At BWC, the
508 ORG simulation agrees well with observations in terms of ALT but the temperature envelopes are
509 generally colder than observed. The M-org configuration at this site results in a talik between 2 and 9m
510 which is not seen in the observations. The minimum envelope is too cold near the surface for ORG
511 configurations at the three sites because of the thermal properties of the peat (Dobinski, 2011; Kujala et
512 al., 2008). This is discussed further in Section 3.5.

513 To aid with the selection of the best configuration for each site, we calculated RMSE for the temperature
514 envelopes (Tmax and Tmin separately) by interpolating the simulation results at the depths of
515 observations, discarding points/years where/when the sensors fail. The available records vary from site
516 to site. The results are shown in Figure 11 for the simulations started after 2000 spin-up cycles with a small
517 inset table on each panel showing how the mean RMSE over the simulation period changes with spin-up
518 cycles. The change in RMSE with cycles is small to negligible. In general, Tmax is better simulated than the
519 Tmin, except for BWC M-org configuration. M-org has lower errors than ORG for HPC while the situation
520 is reversed for HPC (i.e. M-org is better than ORG). For JMR, the performance of the ORG configuration is
521 similar to M-org for Tmax but is better for Tmin. The shape of the Tmin envelope is better. Given the
522 requirement to have generic rules to be applicable at the MRB scale, we prefer to use the ORG
523 configuration at this site. The following sections assess the sensitivity of the results to SDEP, TBOT, and
524 organic depth for the preferred configuration at each site.

525 **Possible Position of Figure 11**

3.3 Impact of Permeable Depth (SDEP)

526 SDEP for the above mentioned configurations for each site was perturbed in the range of 5-15m keeping
527 other studied parameters (TBOT and organic configuration) fixed. Figure 12 shows the impact for each
528 site on the average ALT and DZAA over the analysis period (1980-2016) for all land cover types. 100
529 spinning-up cycles were used to initialize those simulations. The land cover derived GRUs vary between
530 the sites. For JMR, wetlands do not develop permafrost while at shallower SDEP values, taliks (i.e. no
531 permafrost – NPF on the figures) develop under forest GRUs in some years. Thus, the averages shown on
532 Figure 12 are for those years when the soil is cryotic all year round, which varies across the tested SDEP
533 range. There is a general tendency for ALT to slightly decrease with deeper SDEP values for all land cover
534 types, except for grass and shrubs at HPC. SDEP impact on DZAA varies across sites and GRUs. While DZAA
535 increases initially with SDEP at JMR then becomes insensitive, it initially decreases with SDEP for HPC then
536 increases at a slower rate. At BWC it initially decreases with larger SDEP then increases before becoming
537 insensitive to SDEP. DZAA is generally shallower for JMR followed by BWC and then HPC in close
538 correlation with the depth of organic layers. This behaviour may also be correlated to the thickness of
539 permafrost that increases in the same order.

540 **Possible Position of Figure 12**

541 Figure 13(top) shows how these changes to ALT and DZAA are occurring via changes in the shape of the
542 temperature envelopes for a selected year. Increasing SDEP actually allows more cooling of the middle
543 soil layers (between 0.5 – 10m) which pushes the maximum envelope upwards reducing ALT. The
544 envelopes bend again to reach the specified bottom temperature, which is much clearer for JMR (because
545 it is set to +0.80°C) than BWC and HPC where it is set to a negative value. Differences across the SDEP
546 range are small for HPC because of the M-org configuration. The straighter envelopes of HPC tend to meet
547 (i.e. at DZAA) at larger depths than the curved ones at BWC and JMR. This cooling effect is possibly related
548 to having moisture, especially ice, in deeper soil layers with deeper SDEP, which affects the thermal
549 properties of the soil. The presence of ice increases the thermal conductivity of the soil in general,
550 compared to dry soil (see Section S1 in the supplement). The bottom panel of Figure 13 summarizes the
551 impact of SDEP on RMSE for ALT, DZAA, Tmax and Tmin over the simulation periods (years with
552 observations as shown in Figure 11). There are trade-offs in simulating the various aspects as the minimum
553 RMSE values are attained at the maximum SDEP used for Tmin, Tmax and DZAA at JMR and BWC while
554 the minimum RMSE values for ALT is attained at the maximum used SDEP value. Except for ALT, RMSE
555 seem insensitive to SDEP at HPC.

556

Possible Position of Figure 13

3.4 Impact of Bottom Temperature (TBOT)

557 As shown by the spinning-up experiments above, the initial temperature of the deepest layer remains
558 virtually unchanged through the spin-up and thus has to be specified. It was expected that simulations
559 might converge to a possibly different steady state value at the end of spin-up but they did not. The
560 bottom of soil column has a constant flux boundary condition (Section 2.1). We used the default zero
561 value for this constant, implying no gradient at the bottom, while TBOT is only an initial condition for the
562 first spin-up cycle. We also tested values for the geothermal flux of 0.083 Wm^{-2} at the three sites and
563 found negligible impact confirming the previous findings of Sapriz-Azuri et al. (2018). This value for the
564 heat flux is the maximum of the range specified for Western Canada by Garland and Lennox (1962).
565 Temperature observations as deep as 50m are rare and relationships between that temperature and air
566 or near surface soil temperature are neither available nor appropriate. For the studied sites, it has been
567 estimated from the observed profiles, and perturbed within a range (-3.0 to +1.5°C), which was varied
568 depending on the site condition/location. Figure 14 shows the impact of changing the temperature of the
569 deepest layer on ALT and DZAA. For JMR, increasing TBOT increases ALT quickly so that taliks form under
570 wetlands if $\text{TBOT} > 0^\circ\text{C}$ and other land cover types follow at higher temperatures such that permafrost
571 does not develop under most canopy types if $\text{TBOT} > 1.5^\circ\text{C}$. This gives a way to simulate the no permafrost
572 conditions observed at all sites in the basin (except 85-12B-T4). A similar relationship is simulated for BWC
573 as increasing TBOT increases ALT especially for wetlands. ALT at HPC is insensitive to TBOT because of the
574 generally colder conditions and thicker permafrost. DZAA is showing low sensitivity to TBOT except for
575 wetlands at JMR.

576

Possible Position of Figure 14

577 Figure 15(top) shows how the temperature envelopes respond to changes in TBOT. In all cases, the
578 envelopes seem to bend at some depth to try to reach the given bottom temperature. SDEP seems to
579 influence the start of that inflection. This bending towards the given temperature causes another
580 inflection of the maximum envelope closer to the surface. Depending on the depth of that first inflection,
581 ALT may or may not be affected. DZAA is not affected as much but the temperature at DZAA depends on
582 TBOT. There is a noticeable difference between the M-org configuration of HPC on one hand and the ORG
583 configuration at JMR and BWC on the other. Figure 15(bottom) shows the impact of TBOT on model
584 performance as measured by RMSE of ALT, DZAA, Tmin and Tmax. Again we see trade-offs between
585 getting the proper shape for the envelopes (as measured by RMSE for Tmax and Tmin) and the ALT for

586 JMR indicating that a range between 0.5°C to 1.0°C for TBOT gives reasonable performance across the
587 four metrics. For BWC, ALT and DZAA are little sensitive to TBOT a range of -0.5°C to -1°C gives the best
588 overall performance. For HPC, the colder the TBOT, the lower the RMSE values for most metrics, a value
589 around -2°C is reasonable.

590 **Possible Position of Figure 15**

3.5 Impact of Organic Depth (ORG) and Configuration

591 It is believed that organic soils provide insulation to the impacts of the atmosphere on the soil
592 temperature, which would lead to a thinner active layer than in a fully mineral soil. This assumption has
593 been tested for the three sites by changing the depth of the fully organic layers (ORG) for JMR and BWC
594 as well as the mineral layers containing organic content (M-org) at HPC. The results are sometimes
595 counter-intuitive. Peat plateaux are widespread in the JMR region and thus the fully organic layers are
596 followed by layers of high organic content (50%) till SDEP. Increasing the fully organic layers initially
597 reduces ALT (Figure 16) as expected but also reduces DZAA quickly. Then the ALT (which is defined mainly
598 by the maximum temperature envelope) increases again which means that a deeper fully organic layer
599 provides less insulation. The reason is related to the thermal and hydraulic properties of the peat. BWC
600 exhibits different behaviour to JMR as ALT increases initially when increasing the fully organic layers from
601 3 to 4 then decreases gradually. DZAA seems to decrease with increasing the organic depth for most land
602 cover types at the three sites. DZAA and ALT show little sensitivity to the depth organic layers at HPC
603 because the thermal and hydraulic properties under the M-org configuration are affected by the sand and
604 clay fractions while they are set to specific values for fully organic soils (ORG). Wetlands behave in a
605 different way compared to other land cover types at the different sites because they are configured to
606 remain close to saturation as much as possible. At JMR, wetlands are not underlain by permafrost for all
607 organic configurations, which agrees with the literature.

608 **Possible Position of Figure 16**

609 Figure 17(top) shows the response of the temperature envelopes to changes in the organic depth.
610 Increasing the organic depth causes much larger negative temperatures near the surface for the minimum
611 envelope for ORG but causes the inflection of the minimum envelope to occur at slightly higher
612 temperatures. A similar, but smaller, effect can be seen for the maximum envelope. The maximum
613 envelopes for the different organic depth intersect, which corroborates with the above results for ALT.
614 Another interesting feature can be observed comparing the ORG and M-org configurations. The M-org

615 configurations has a much smaller temperature range near the surface than the fully organic soil and
616 causes less cooling in the intermediate soil layers (above SDEP) such that the observed profiles are better
617 matched HPC. The high thermal capacity of the peat combined with its high thermal conductivity when
618 containing ice in winter cause this cooling at the surface (Dobinski, 2011).

619 Figure 17(bottom) summarizes the impact of organic depth (ORG for JMR and BWC, and M-org for HPC)
620 on the RMSE of ALT, DZAA, and the temperature envelopes. The impact in JMR is interesting as there are
621 clear optimal values for ALT and Tmin and, to some extent, Tmax, although the optimal value is not the
622 same for each aspect, leading to trade-offs. The selected 1.46m depth (8 ORG layers) provides the best
623 performance overall. For BWC, RMSE for Tmax and Tmin move in opposite directions (Tmin RMSE
624 generally reduces while Tmax RMSE increases with deeper ORG). A depth around 0.5m is generally
625 satisfactory. For HPC, depths containing organic matter less than 0.6m provide the optimal performance
626 across the different aspects. A multi-criteria calibration framework can be setup using those performance
627 metrics if the aim is the find the best configuration (including SDEP and TBOT) for each site. However, we
628 are seeking generic rules that can be applied at larger scales, such as that of the MRB as a whole.

629 **Possible Position of Figure 17**

4. Discussion and Conclusions

630 Permafrost is an important feature of cold regions, such as the Mackenzie River Basin, and needs to be
631 properly represented in land surface hydrological models, especially under the unprecedented climate
632 warming trends that have been observed in these regions. The current generation of LSMs is being
633 improved to simulate permafrost dynamics by allowing deeper soil profiles than typically used and
634 incorporating organic soils explicitly. Deeper soil profiles have larger hydraulic and thermal memories that
635 require more effort to initialize. We followed the recommendations of previous studies (e.g. Lawrence et
636 al., 2012; Sapriza-Azuri et al., 2018) to select the total soil column depth to be around 50m. The
637 temperature envelopes meet (at DZAA) well within the 50m soil column over the simulation period
638 (including spinning-up), such that the bottom boundary condition is not disturbing the simulated
639 temperature profiles/envelopes and ALT.

640 We analysed the conventional layering schemes used by other LSMs, which tend to use an exponential
641 formulation to maximize the number of layers near the surface and minimize the total number of layers
642 (Oleson et al., 2013; Park et al., 2014). We found that the exponential formulation is not adequate to
643 capture the dynamics of the active layer depth and thus tested two other alternative schemes that have

644 smaller thicknesses for the first 2 meters, instead of the conventional ones. The first scheme (SC1) had
645 equally-sized layers in the first 1m, followed by thicker but equally-sized layers in the second 1m. The
646 second scheme (SC2) was formulated to have increasing thicknesses with depth following a scaled power
647 law, which we found to be more suitable for the explicit forward numerical solution used by CLASS.

648 We discussed the common initialization approaches, including spinning up the model repeatedly using a
649 single year (e.g. Dankers et al., 2011; Nishimura et al., 2009) or a sequence of years (e.g. Park et al., 2013),
650 spinning up the model in a transient condition on long paleo-climatic records (e.g. Ednie et al., 2008), or
651 combining both of these approaches (Sapriza-Azuri et al., 2018). Paleo-climatic reconstructions are scarce
652 and provide limited information (e.g. mean summer temperature or total annual precipitation), while
653 LSMs typically require a suite of meteorological variables at a high temporal resolution for the whole study
654 domain. These variables can be stochastically generated at the resolution of interest informed by paleo-
655 records. However, such practice is computationally expensive, especially for large domains and also
656 introduces additional uncertainties. The approach of spinning-up using available 20th century data has
657 been criticized as picking up the anthropogenic climate warming signal that started around 1850 and thus
658 would yield initial conditions that are not representative. However, paleo climatic records also show that
659 the climate has always been transient and there may not exist a long enough period of quasi-equilibrium
660 to start the spinning-up process (Razavi et al., 2015). Spinning-up using a sequence of years is thus more
661 prone to having a trend than a single year and de-trending the sequence is not free of assumptions either.

662 Given the above complications, we investigated the impact of the simplest approach, which is spinning-
663 up using a single year (similar to Burke et al., 2013; Dankers et al., 2011), on several permafrost metrics
664 (active layer depth – ALT, depth of zero annual amplitude – DZAA, and annual temperature envelopes).
665 The aim was to determine the minimum number of spinning-up cycles to have satisfactory performance
666 (if reached) and to know how much accuracy is lost by not spinning more. We did this for three sites along
667 a south-north transect in the Mackenzie River Valley sampling the different permafrost zones (sporadic,
668 extensive discontinuous and continuous) in order to be able to generalize the findings to the whole MRB
669 domain. Additionally, we investigated the sensitivity of the results to some important parameters such as
670 the depth to bedrock (SDEP), the temperature of the deepest layer (TBOT), and the organic soil
671 configuration (ORG).

672 The results show that temperature profiles at the end of spinning cycles remained virtually unchanged
673 (i.e. reached a quasi steady state) after 50-100 cycles, when benchmarked against the results of 2000
674 cycles. We focused on temperature profiles for this stability analysis, because we found that the soil

675 moisture profiles (both liquid and frozen) stabilize much earlier during spin-up. In some cases, changes in
676 the middle layers occurred after 100 cycles but the influence of that on the simulated envelopes, ALT and
677 DZAA was found to be small to negligible compared to the uncertainty of observations and the scale of
678 our model. We also found that the selection of the layering scheme has an effect on stabilization and our
679 proposed scheme (SC2) with increasing thicknesses with depth reached stability faster and had less
680 drifting. Therefore, the simple single-year spinning approach seems to be sufficient for our purpose using
681 SC2. This agrees with Dankers et al. (2011) who showed that a higher vertical resolution improved the
682 simulation of ALT using JULES.

683 We also found that the temperature of the deepest soil layer (TBOT) remained virtually unchanged from
684 the specified initial value even after 2000 spinning cycles. Therefore, this temperature has to be specified
685 by the modeller. For the study sites, we extrapolated it from the observed envelopes and studied the
686 effect of perturbing it around the extrapolated value. This perturbation had small impacts on ALT and
687 DZAA except for JMR which is located in the sporadic permafrost zone, but it had a significant impact on
688 the shape of the envelopes. Temperature observations going as deep as 50m are rare. Most of the
689 permafrost monitoring sites in the MRB have up to 20m cables and thus we do not know whether the
690 temperature of deeper soil layers has been changing over time, and if so, by how much. Changes in
691 temperature at the deepest sensors at each of the three sites can be seen in Figure S1 of the
692 supplementary material. To take the information back to the large scale, we recommend using a south to
693 north gradient moving from +1.0 in the sporadic zone to -2.0 in the continuous zone and specifying a
694 spatially variable field as an input initial condition. These effects show the regional variability which needs
695 to be assessed for different applications such as other basins affected by permafrost, or using other LSMs.
696 This could lead to the verification of such finding and to the preparation of a global map of initial values
697 for TBOT by combining observations and modelling. We have not seen such detailed analyses in the
698 literature.

699 For this study, we tested whether a non-zero thermal flux boundary condition could resolve this issue but
700 the impacts were negligible using the literature values for the geothermal flux (0.083 Wm^{-2}) in the region.
701 However, available datasets for the geothermal flux (e.g. Bachu, 1993) are not transient and estimate
702 those fluxes at depths greater than the 50m used. Our results agree with those of Nishimura et al. (2009)
703 and Sapriz-Azuri et al. (2018) who showed that the geothermal heat flux had negligible effect on most
704 simulations in study areas in Siberia and Canada respectively. Nevertheless, the issue may need further

705 investigation using other models (including thermal ones) and tests in other regions before generalizing
706 such conclusion.

707 The analyses also demonstrated the importance of the organic soil configuration (i.e. number of layers
708 and their parameterization respective of organic sub-types) on the simulated temperature profiles and
709 active layer dynamics. This has been illustrated in the literature. For example, Dankers et al. (2011) found
710 that adjusting soil parameters for organic content to have relatively little effect on ALT simulations of the
711 Arctic region while Nicolsky et al. (2007) and Park et al. (2013) stressed the importance of organic content
712 to the fidelity of permafrost simulations. Park et al. (2013) further indicated that organic matter evolves
713 dynamically as it decomposes over time and depends on biogeochemical processes such as plant growth,
714 root development, and littering. This could be simulated in LSMs by including the carbon cycle. However,
715 fully organic soils were not extensively tested in permafrost context as shown in our study.

716 In most cases, we found combinations of TBOT, SDEP, and ORG that produced satisfactory simulations but
717 the impact of organic layering seems to require further investigation, as increasing the thickness of organic
718 layers does not always act to reduce ALT or reduce the cooling in the middle soil layers that should result
719 from increased insulation. There is an interplay between the moisture properties/content and thermal
720 properties of organic soils that needs further investigation. Additionally, we cannot represent stacked
721 canopies using CLASS, e.g. trees or shrubs underlain by moss or the effect of litter under (deciduous)
722 trees/shrubs. Moss or litter could be providing additional insulation under those canopies that is not
723 represented. The quality of snow simulations can also impact the quality of permafrost simulations. For
724 example, Burke et al. (2013) showed that a multi-layer snow model improved ALT simulations in JULES;
725 CLASS has a single layer snow model.

726 To conclude, we have formulated a generic approach to represent permafrost within the MESH
727 framework (running CLASS) for applications at large scales that has the following features:

728 - A 50m deep soil profile with increasing soil thickness with depth;
729 - 50-100 Spinning cycles of the first year of record to initialize the moisture and temperature
730 profiles; and
731 - Spatially distributed TBOT, SDEP, and soil texture parameters, with a systematic guideline to use
732 the 30% threshold to identify fully organic soils.

733 The generic nature of this approach comes from testing it at three sites within different permafrost classes
734 (sporadic, discontinuous and continuous). However, testing the approach is other regions, and with other

735 LSMs (e.g. CLM, MESH/SVS), is necessary before pursuing it for wider applications. This can be done using
736 representative sub-basins where permafrost observations exist to test the above mentioned elements
737 and make any necessary adjustments for application at large scales. Additionally, this study demonstrated
738 a simple and effective way to use small-scale investigations to inform larger scale modelling. While the
739 GRU-based parameterization approach facilitates such transferability, the key is to use the same physics
740 at both scales.

741 It was necessary to increase the flexibility of the MESH framework to accommodate these input formats
742 as well as to produce relevant permafrost outputs. However, the model is still deficient in some ways. For
743 example, the explicit forward numerical solution may limit how soil layering should be defined. The lack
744 of complex canopies, the use of a single layer snow model, and the static nature of soil organic content
745 may be affecting our parameterization of MESH. The parameterization of bedrock as sandstone requires
746 further investigation as it does not reflect the spatial variability of thermal properties of bedrock material.
747 These findings are not specific to MESS/CLASS and could be beneficial for the LSM community in general.
748 Therefore, further analysis and model development is required towards improving the realism of the
749 simulations in permafrost regions. It is vitally required to incorporate key features of permafrost dynamics
750 (e.g. taliks, land subsidence, and thermokarst) into LSMs, as well as the linkages between permafrost
751 evolution phase (aggradation/degradation) and carbon-climate feedback cycles under the changing
752 climatic conditions. The inclusion of such features could enhance the representation of hydrological
753 processes within LSMs and, consequently, ESMs. Accordingly, there is a pressing need to promote
754 multidisciplinary research in permafrost territories among hydrologists, climatologists, geomorphologists,
755 and geotechnical engineers.

Acknowledgements

756 This research was undertaken as part of the Changing Cold Region Network, funded by Canada's Natural
757 Science and Engineering Research Council and by the Canada Excellence Research Chair in Water Security
758 at the University of Saskatchewan. We gratefully acknowledge the contribution of two anonymous
759 reviewers to the improvement of the manuscript.

Author Contributions

760 M.E., A.P. and H.W. conceived the experimental design of this study. G.S.-A. provided the original MESH
761 setup of the MRB. G.S.-A. and M.E. collected the permafrost observations. D.P. provided the MESH code
762 and implemented the necessary code changes. M.E. conducted the simulation work and analysed the
763 results. M.A. participated in the interpretation of results and preparation of some illustrations. M.E.
764 prepared the manuscript with contributions from all co-authors.

Competing Interests

765 The authors declare that they have no conflict of interest.

Code and Data Availability

766 MESH code is available from the MESH wiki page (<https://wiki.usask.ca/display/MESH/Releases>).
767 Distributed soil texture and SDEP data are available from Keshav et al. (2019b, 2019a). Permafrost
768 observations were collected from various reports of Geological Survey Canada as referenced in the
769 manuscript.

References

770 Alexeev, V. A., Nicolsky, D. J., Romanovsky, V. E. and Lawrence, D. M.: An evaluation of deep soil
771 configurations in the CLM3 for improved representation of permafrost, *Geophys. Res. Lett.*, 34(9),
772 doi:10.1029/2007GL029536, 2007.
773 Arboleda-Obando, P.: Determinando los efectos del cambio climático y del cambio en usos del suelo en la
774 Macro Cuenca Magdalena Cauca utilizando el modelo de suelo-superficie e hidrológico MESH. [online]
775 Available from: <http://bdigital.unal.edu.co/69823/1/1018438123.2018.pdf> (Accessed 18 April 2019),
776 2018.

777 Bachu, S.: Basement heat flow in the Western Canada Sedimentary Basin, *Tectonophysics*, 222(1), 119–
778 133, doi:10.1016/0040-1951(93)90194-O, 1993.

779 Bahremand, A., Razavi, S., Pietroniro, A., Haghnegahdar, A., Princz, D., Gharari, S., Elshamy, M. and
780 Tesemma, Z.: Application of MESH Land Surface-Hydrology Model to a Large River Basin in Iran Model
781 Prospective works, in Canadian Geophysical Union General Assembly 2018, p. 3, Niagara Falls., 2018.

782 Best, M. J., Pryor, M., Clark, D. B., Rooney, G. G., Essery, R. L. H., Ménard, C. B., Edwards, J. M., Hendry, M.
783 A., Porson, A., Gedney, N., Mercado, L. M., Sitch, S., Blyth, E., Boucher, O., Cox, P. M., Grimmond, C. S. B.
784 and Harding, R. J.: The Joint UK Land Environment Simulator (JULES), model description-Part 1: Energy and
785 water fluxes, *Geosci. Model Dev*, 4, 677–699, doi:10.5194/gmd-4-677-2011, 2011.

786 Bonsal, B. R., Peters, D. L., Seglenieks, F., Rivera, A. and Berg, A.: Changes in freshwater availability across
787 Canada, in Canada's Changing Climate Report, pp. 261–342. [online] Available from:
788 <https://www.nrcan.gc.ca/sites/www.nrcan.gc.ca/files/energy/Climate-change/pdf/CCCR-Chapter6-ChangesInFreshwaterAvailabilityAcrossCanada.pdf> (Accessed 27 August 2019), 2019.

790 Burke, E. J., Dankers, R., Jones, C. D. and Wiltshire, A. J.: A retrospective analysis of pan Arctic permafrost
791 using the JULES land surface model, *Clim. Dyn.*, 41(3–4), 1025–1038, doi:10.1007/s00382-012-1648-x,
792 2013.

793 Burn, C. R. and Nelson, F. E.: Comment on “A projection of severe near-surface permafrost degradation
794 during the 21st century” by David M. Lawrence and Andrew G. Slater, *Geophys. Res. Lett.*, 33(21), L21503,
795 doi:10.1029/2006gl027077, 2006.

796 Calmels, F., Laurent, C., Brown, R., Pivot, F. and Ireland, M.: How Permafrost Thaw May Impact Food
797 Security of Jean Marie River First Nation, NWT, *GeoQuebec 2015 Conf. Pap.*, (September), 2015.

798 Canada Centre for Remote Sensing (CCRS), Nacional para el Conocimiento y Uso de la Biodiversidad
799 (CONABIO), Comisión Nacional Forestal (CONAFOR), Instituto Nacional de Estadística y Geografía (INEGI)
800 and U.S. Geological Survey (USGS): 2005 North American Land Cover at 250 m spatial resolution, [online]
801 Available from: <http://www.cec.org/tools-and-resources/map-files/land-cover-2005>, 2010.

802 Changwei, X. and Gough, W. A.: A Simple Thaw-Freeze Algorithm for a Multi-Layered Soil using the Stefan
803 Equation, *Permafro. Periglac. Process.*, 24(3), 252–260, doi:10.1002/ppp.1770, 2013.

804 Côté, J., Gravel, S., Méthot, A., Patoine, A., Roch, M., Staniforth, A., Côté, J., Gravel, S., Méthot, A., Patoine,

805 A., Roch, M. and Staniforth, A.: The Operational CMC–MRB Global Environmental Multiscale (GEM)
806 Model. Part I: Design Considerations and Formulation, *Mon. Weather Rev.*, 126(6), 1373–1395,
807 doi:10.1175/1520-0493(1998)126<1373:TOCMGE>2.0.CO;2, 1998a.

808 Côté, J., Desmarais, J.-G., Gravel, S., Méthot, A., Patoine, A., Staniforth, A. and Roch, M.: The Operational
809 CMC – MRB Global Environmental Multiscale (GEM) Model . Part II : Results, *Mon. Weather Rev.*, 126(6),
810 1397–1418, doi:[http://dx.doi.org/10.1175/1520-0493\(1998\)126<1397:TOCMGE>2.0.CO;2](http://dx.doi.org/10.1175/1520-0493(1998)126<1397:TOCMGE>2.0.CO;2), 1998b.

811 Dankers, R., Burke, E. J. and Price, J.: Simulation of permafrost and seasonal thaw depth in the JULES land
812 surface scheme, *Cryosphere*, 5(3), 773–790, doi:10.5194/tc-5-773-2011, 2011.

813 DeBeer, C. M., Wheater, H. S., Carey, S. K. and Chun, K. P.: Recent climatic, cryospheric, and hydrological
814 changes over the interior of western Canada: a review and synthesis, *Hydrol. Earth Syst. Sci.*, 20(4), 1573–
815 1598, doi:10.5194/hess-20-1573-2016, 2016.

816 Dobinski, W.: Permafrost, *Earth-Science Rev.*, 108(3–4), 158–169, doi:10.1016/J.EARSCIREV.2011.06.007,
817 2011.

818 Duan, L., Man, X., Kurylyk, B. L. and Cai, T.: Increasing winter baseflow in response to permafrost thaw
819 and precipitation regime shifts in northeastern China, *Water (Switzerland)*, 9(1), 25,
820 doi:10.3390/w9010025, 2017.

821 Durocher, M., Requena, A. I., Burn, D. H. and Pellerin, J.: Analysis of trends in annual streamflow to the
822 Arctic Ocean, *Hydrol. Process.*, 33(7), 1143–1151, doi:10.1002/hyp.13392, 2019.

823 Ednie, M., Wright, J. F. and Duchesne, C.: Establishing initial conditions for transient ground thermal
824 modeling in the Mackenzie Valley: a paleo-climatic reconstruction approach, in *Proceedings of the Ninth*
825 *International Conference on Permafrost*, edited by D. L. Kane and H. K. M., pp. 403–408, *Institute of*
826 *Northern Engineering, University of Alaska Fairbanks, Fairbanks, Alaska.*, 2008.

827 van Everdingen, R. O.: *Glossary of Permafrost and Related Ground-Ice Terms.*, 2005.

828 Garland, G. D. and Lennox, D. H.: Heat Flow in Western Canada, *Geophys. J. R. Astron. Soc.*, 6(2), 245–262,
829 doi:10.1111/j.1365-246X.1962.tb02979.x, 1962.

830 Haghnegahdar, A., Tolson, B. A., Craig, J. R. and Paya, K. T.: Assessing the performance of a semi-
831 distributed hydrological model under various watershed discretization schemes, *Hydrol. Process.*, 29(18),
832 4018–4031, doi:10.1002/hyp.10550, 2015.

833 Hegginbottom, J. A., Dubreuil, M. A. and Harker, P. T.: Permafrost, in National Atlas of Canada, p. MCR
834 4177, Natural Resources Canada., 1995.

835 Husain, S. Z., Alavi, N., Bélair, S., Carrera, M., Zhang, S., Fortin, V., Abrahamowicz, M., Gauthier, N., Husain,
836 S. Z., Alavi, N., Bélair, S., Carrera, M., Zhang, S., Fortin, V., Abrahamowicz, M. and Gauthier, N.: The
837 Multibudget Soil, Vegetation, and Snow (SVS) Scheme for Land Surface Parameterization: Offline Warm
838 Season Evaluation, *J. Hydrometeorol.*, 17(8), 2293–2313, doi:10.1175/JHM-D-15-0228.1, 2016.

839 IPCC: Climate Change 2014 Impacts, Adaptation, and Vulnerability Part B: Regional Aspects, edited by V.
840 R. Barros, C. B. Field, D. J. Dokken, M. D. Mastrandrea, K. J. Mach, T. E. Bilir, M. Chatterjee, K. L. Ebi, Y. O.
841 Estrada, R. C. Genova, B. Girma, E. S. Kissel, A. N. Levy, S. MacCracken, P. R. Mastrandrea, and L. L. White,
842 Cambridge University Press, Cambridge, United Kingdom and New York, NY, USA., 2014.

843 St. Jacques, J. M. and Sauchyn, D. J.: Increasing winter baseflow and mean annual streamflow from
844 possible permafrost thawing in the Northwest Territories, Canada, *Geophys. Res. Lett.*, 36(1), L01401,
845 doi:10.1029/2008GL035822, 2009.

846 Keshav, K., Haghnegahdar, A., Elshamy, M., Gharari, S. and Razavi, S.: Aggregated gridded soil texture
847 dataset for Mackenzie and Nelson-Churchill River Basins, , doi:<https://dx.doi.org/10.20383/101.0154>,
848 2019a.

849 Keshav, K., Haghnegahdar, A., Elshamy, M., Gharari, S. and Razavi, S.: Bedrock depth dataset for Nelson-
850 Churchill and Mackenzie River Basin based on bedrock data by Shangguan et al. (2016), ,
851 doi:<https://dx.doi.org/10.20383/101.0152>, 2019b.

852 Kouwen, N.: WATFLOOD: a Micro-Computer Based Flood Forecasting System Based on Real-Time Weather
853 Radar, *Can. Water Resour. J.*, 13(1), 62–77, doi:10.4296/cwrj1301062, 1988.

854 Kouwen, N., Soulis, E. D., Pietroniro, A., Donald, J. and Harrington, R. A.: Grouped Response Units for
855 Distributed Hydrologic Modeling, *J. Water Resour. Plan. Manag.*, 119(3), 289–305,
856 doi:10.1061/(ASCE)0733-9496(1993)119:3(289), 1993.

857 Krogh, S. A., Pomeroy, J. W. and Marsh, P.: Diagnosis of the hydrology of a small Arctic basin at the tundra-
858 taiga transition using a physically based hydrological model, *J. Hydrol.*, 550(May), 685–703,
859 doi:10.1016/j.jhydrol.2017.05.042, 2017.

860 Kujala, K., Seppälä, M. and Holappa, T.: Physical properties of peat and palsa formation, *Cold Reg. Sci.*

861 Technol., 52(3), 408–414, doi:10.1016/j.coldregions.2007.08.002, 2008.

862 Lawrence, D. M. and Slater, A. G.: A projection of severe near-surface permafrost degradation during the
863 21st century, *Geophys. Res. Lett.*, 32(24), L24401, doi:10.1029/2005GL025080, 2005.

864 Lawrence, D. M., Slater, A. G., Romanovsky, V. E. and Nicolsky, D. J.: Sensitivity of a model projection of
865 near-surface permafrost degradation to soil column depth and representation of soil organic matter, *J.*
866 *Geophys. Res. Earth Surf.*, 113(2), 1–14, doi:10.1029/2007JF000883, 2008.

867 Lawrence, D. M., Slater, A. G. and Swenson, S. C.: Simulation of present-day and future permafrost and
868 seasonally frozen ground conditions in CCSM4, *J. Clim.*, 25(7), 2207–2225, doi:10.1175/JCLI-D-11-00334.1,
869 2012.

870 Letts, M. G., Roulet, N. T., Comer, N. T., Skarupa, M. R. and Verseghy, D. L.: Parameterization of Peatland
871 Hydraulic Properties for the Canadian Land Surface Scheme, *ATMOSPHERE-OCEAN*, 38(1),
872 doi:10.1080/07055900.2000.9649643, 2000.

873 Luo, Y., Arnold, J., Allen, P. and Chen, X.: Baseflow simulation using SWAT model in an inland river basin
874 in Tianshan Mountains, Northwest China, *Hydrol. Earth Syst. Sci.*, 16(4), 1259–1267, doi:10.5194/hess-16-
875 1259-2012, 2012.

876 Mahfouf, J.-F., Brasnett, B. and Gagnon, S.: A Canadian Precipitation Analysis (CaPA) Project: Description
877 and Preliminary Results, *Atmosphere-Ocean*, 45(1), 1–17, doi:10.3137/ao.v450101, 2007.

878 McBean, G., Alekseev, G., Chen, D., Førland, E., Fyfe, J., Groisman, P. Y., King, R., Melling, H., Vose, R. and
879 H. Whitfield, P.: Arctic Climate: Past and Present Lead, in *Impacts of a Warming Arctic: Arctic Climate*
880 *Impact Assessment*, p. 140., 2005.

881 Nicolsky, D. J., Romanovsky, V. E., Alexeev, V. A. and Lawrence, D. M.: Improved modeling of permafrost
882 dynamics in a GCM land-surface scheme, *Geophys. Res. Lett.*, 34(8), 2–6, doi:10.1029/2007GL029525,
883 2007.

884 Nishimura, S., Martin, C. J., Jardine, R. J. and Fenton, C. H.: A new approach for assessing geothermal
885 response to climate change in permafrost regions, *Geotechnique*, 59(3), 213–227,
886 doi:10.1680/geot.2009.59.3.213, 2009.

887 Oleson, K. W., Lawrence, D. M., Bonan, G. B., Drewsniak, B., Huang, M., Charles, D., Levis, S., Li, F., Riley,
888 W. J., Zachary, M., Swenson, S. C., Thornton, P. E., Bozbayik, A., Fisher, R., Heald, C. L., Kluzek, E., Lamarque,

889 F., Lawrence, P. J., Leung, L. R., Muszala, S., Ricciuto, D. M. and Sacks, W.: Technical Description of version
890 4.5 of the Community Land Model (CLM) Coordinating., 2013.

891 Park, H., Iijima, Y., Yabuki, H., Ohta, T., Walsh, J., Kodama, Y. and Ohata, T.: The application of a coupled
892 hydrological and biogeochemical model (CHANGE) for modeling of energy, water, and CO₂ exchanges
893 over a larch forest in eastern Siberia, *J. Geophys. Res.*, 116(D15), D15102, doi:10.1029/2010JD015386,
894 2011.

895 Park, H., Walsh, J., Fedorov, A. N., Sherstiukov, A. B., Iijima, Y. and Ohata, T.: The influence of climate and
896 hydrological variables on opposite anomaly in active-layer thickness between Eurasian and North
897 American watersheds, *Cryosph.*, 7(2), 631–645, doi:10.5194/tc-7-631-2013, 2013.

898 Park, H., Sherstiukov, A. B., Fedorov, A. N., Polyakov, I. V. and Walsh, J. E.: An observation-based
899 assessment of the influences of air temperature and snow depth on soil temperature in Russia, *Environ.*
900 *Res. Lett.*, 9(6), 064026, doi:10.1088/1748-9326/9/6/064026, 2014.

901 Pietroniro, A., Fortin, V., Kouwen, N., Neal, C., Turcotte, R., Davison, B., Verseghy, D., Soulis, E. D., Caldwell,
902 R., Evora, N. and Pellerin, P.: Development of the MESH modelling system for hydrological ensemble
903 forecasting of the Laurentian Great Lakes at the regional scale, *Hydrol. Earth Syst. Sci.*, 11(4), 1279–1294,
904 doi:10.5194/hess-11-1279-2007, 2007.

905 Pomeroy, J. W., Gray, D. M., Brown, T., Hedstrom, N. R., Quinton, W. L., Granger, R. J. and Carey, S. K.: The
906 cold regions hydrological model: a platform for basing process representation and model structure on
907 physical evidence, *Hydrol. Process.*, 21(19), 2650–2667, doi:10.1002/hyp.6787, 2007.

908 Quinton, W. L. and Marsh, P.: A conceptual framework for runoff generation in a permafrost environment,
909 *Hydrol. Process.*, 13(16), 2563–2581, doi:10.1002/(SICI)1099-1085(199911)13:16<2563::AID-
910 HYP942>3.0.CO;2-D, 1999.

911 Quinton, W. L., Hayashi, M. and Chasmer, L. E.: Permafrost-thaw-induced land-cover change in the
912 Canadian subarctic: implications for water resources, *Hydrol. Process.*, 25(1), 152–158,
913 doi:10.1002/hyp.7894, 2011.

914 Razavi, S., Elshorbagy, A., Wheater, H. and Sauchyn, D.: Toward understanding nonstationarity in climate
915 and hydrology through tree ring proxy records, *Water Resour. Res.*, 51(3), 1813–1830,
916 doi:10.1002/2014WR015696, 2015.

917 Riseborough, D., Shiklomanov, N., Etzelmüller, B., Gruber, S. and Marchenko, S.: Recent advances in
918 permafrost modelling, *Permafro. Periglac. Process.*, 19(2), 137–156, doi:10.1002/ppp.615, 2008.

919 Romanovsky, V. E. and Osterkamp, T. E.: Interannual variations of the thermal regime of the active layer
920 and near-surface permafrost in northern Alaska, *Permafro. Periglac. Process.*, 6(4), 313–335,
921 doi:10.1002/ppp.3430060404, 1995.

922 Sapriza-Azuri, G., Gamazo, P., Razavi, S. and Wheater, H. S.: On the appropriate definition of soil profile
923 configuration and initial conditions for land surface–hydrology models in cold regions, *Hydrol. Earth Syst.
924 Sci.*, 22(6), 3295–3309, doi:10.5194/hess-22-3295-2018, 2018.

925 Shangguan, W., Hengl, T., Mendes de Jesus, J., Yuan, H. and Dai, Y.: Mapping the global depth to bedrock
926 for land surface modeling, *J. Adv. Model. Earth Syst.*, 9(1), 65–88, doi:10.1002/2016MS000686, 2017.

927 Sheffield, J., Goteti, G. and Wood, E. F.: Development of a 50-year high-resolution global dataset of
928 meteorological forcings for land surface modeling, *J. Clim.*, 19(13), 3088–3111, doi:10.1175/JCLI3790.1,
929 2006.

930 Smith, S. L. and Burgess, M.: Ground Temperature Database for Northern Canada, 2000.

931 Smith, S. L. and Burgess, M. M.: A digital database of permafrost thickness in Canada., 2002.

932 Smith, S. L., Burgess, M. M., Riseborough, D., Coultsish, T. and Chartrand, J.: Digital summary database of
933 permafrost and thermal conditions - Norman Wells pipeline study sites, Geol. Surv. Canada, Open File
934 4635, 4635, 1–104, doi:10.4095/215482, 2004.

935 Smith, S. L., Ye, S. and Ednie, M.: Enhancement of permafrost monitoring network and collection of
936 baseline environmental data between Fort Good Hope and Norman Wells, Northwest Territories, GSC
937 Curr. Res., 2007.

938 Smith, S. L., Riseborough, D. W., Nixon, F. M., Chartrand, J., Duchesne, C. and Ednie, M.: Data for Geological
939 Survey of Canada Active Layer Monitoring Sites in the Mackenzie Valley , N.W.T., 2009.

940 Smith, S. L., Chartrand, J., Duchesne, C. and Ednie, M.: Report on 2015 field activities and collection of
941 ground thermal and active layer data in the Mackenzie corridor, Northwest Territories, Geol. Surv. Canada
942 Open File 8125, doi:10.4095/292864, 2016.

943 Soulis, E. D. E., Snelgrove, K. K. R., Kouwen, N., Seglenieks, F. and Verseghy, D. L. D.: Towards closing the
944 vertical water balance in Canadian atmospheric models: Coupling of the land surface scheme class with

945 the distributed hydrological model watflood, *Atmosphere-Ocean*, 38(1), 251–269,
946 doi:10.1080/07055900.2000.9649648, 2000.

947 Swenson, S. C., Lawrence, D. M. and Lee, H.: Improved simulation of the terrestrial hydrological cycle in
948 permafrost regions by the Community Land Model, *J. Adv. Model. Earth Syst.*, 4(8), 1–15,
949 doi:10.1029/2012MS000165, 2012.

950 Szeicz, J. M. and MacDonald, G. M.: Dendroclimatic Reconstruction of Summer Temperatures in
951 Northwestern Canada since A.D. 1638 Based on Age-Dependent Modeling, *Quat. Res.*, 44(02), 257–266,
952 doi:10.1006/qres.1995.1070, 1995.

953 Verseghy, D.: CLASS – The Canadian land surface scheme (version 3.6) - technical documentation, Intern.
954 report, Clim. Res. Div. Sci. Technol. Branch, Environ. Canada, (February), 2012.

955 Verseghy, D. L.: Class—A Canadian land surface scheme for GCMS. I. Soil model, *Int. J. Climatol.*, 11(2),
956 111–133, doi:10.1002/joc.3370110202, 1991.

957 Walvoord, M. A. and Kurylyk, B. L.: Hydrologic Impacts of Thawing Permafrost—A Review, *Vadose Zo. J.*,
958 15(6), 0, doi:10.2136/vzj2016.01.0010, 2016.

959 Walvoord, M. A. and Striegl, R. G.: Increased groundwater to stream discharge from permafrost thawing
960 in the Yukon River basin: Potential impacts on lateral export of carbon and nitrogen, *Geophys. Res. Lett.*,
961 34(12), L12402, doi:10.1029/2007GL030216, 2007.

962 Weedon, G. P., Gomes, S., Viterbo, P., Shuttleworth, W. J., Blyth, E., Österle, H., Adam, J. C., Bellouin, N.,
963 Boucher, O. and Best, M.: Creation of the WATCH Forcing Data and Its Use to Assess Global and Regional
964 Reference Crop Evaporation over Land during the Twentieth Century, *J. Hydrometeorol.*, 12(5), 823–848,
965 doi:10.1175/2011JHM1369.1, 2011.

966 Weedon, G. P., Balsamo, G., Bellouin, N., Gomes, S., Best, M. J. and Viterbo, P.: The WFDEI meteorological
967 forcing data set: WATCH Forcing Data methodology applied to ERA-Interim reanalysis data, *Water Resour.*
968 Res., 50, 7505–7514, doi:10.1002/2014WR015638. Received, 2014.

969 Wong, J. S., Razavi, S., Bonsal, B. R., Wheater, H. S. and Asong, Z. E.: Inter-comparison of daily precipitation
970 products for large-scale hydro-climatic applications over Canada, *Hydrol. Earth Syst. Sci.*, 21(4), 2163–
971 2185, doi:10.5194/hess-21-2163-2017, 2017.

972 Wright, J. F., Duchesne, C. and Côté, M. M.: Regional-scale permafrost mapping using the TTOP ground

973 temperature model, in Proceedings 8th International Conference on Permafrost, pp. 1241–1246. [online]
974 Available from: http://research.iarc.uaf.edu/NICOP/DVD/ICOP_2003_Permafrost/Pdf/Chapter_218.pdf
975 (Accessed 19 April 2019), 2003.

976 Yassin, F., Razavi, S., Wheater, H., Sapriz-Azuri, G., Davison, B. and Pietroniro, A.: Enhanced identification
977 of a hydrologic model using streamflow and satellite water storage data: A multicriteria sensitivity analysis
978 and optimization approach, *Hydrol. Process.*, 31(19), 3320–3333, doi:10.1002/hyp.11267, 2017.

979 Yassin, F., Razavi, S., Wong, J. S., Pietroniro, A. and Wheater, H.: Hydrologic-Land Surface Modelling of a
980 Complex System under Precipitation Uncertainty: A Case Study of the Saskatchewan River Basin, Canada,
981 *Hydrol. Earth Syst. Sci. Discuss.*, 1–40, doi:10.5194/hess-2019-207, 2019a.

982 Yassin, F., Razavi, S., Elshamy, M., Davison, B., Sapriz-Azuri, G. and Wheater, H.: Representation and
983 improved parameterization of reservoir operation in hydrological and land-surface models, *Hydrol. Earth
984 Syst. Sci.*, 23(9), 3735–3764, doi:10.5194/hess-23-3735-2019, 2019b.

985 Yeh, K.-S., Côté, J., Gravel, S., Méthot, A., Patoine, A., Roch, M., Staniforth, A., Yeh, K.-S., Côté, J., Gravel,
986 S., Méthot, A., Patoine, A., Roch, M. and Staniforth, A.: The CMC–MRB Global Environmental Multiscale
987 (GEM) Model. Part III: Nonhydrostatic Formulation, *Mon. Weather Rev.*, 130(2), 339–356,
988 doi:10.1175/1520-0493(2002)130<0339:TCMGEM>2.0.CO;2, 2002.

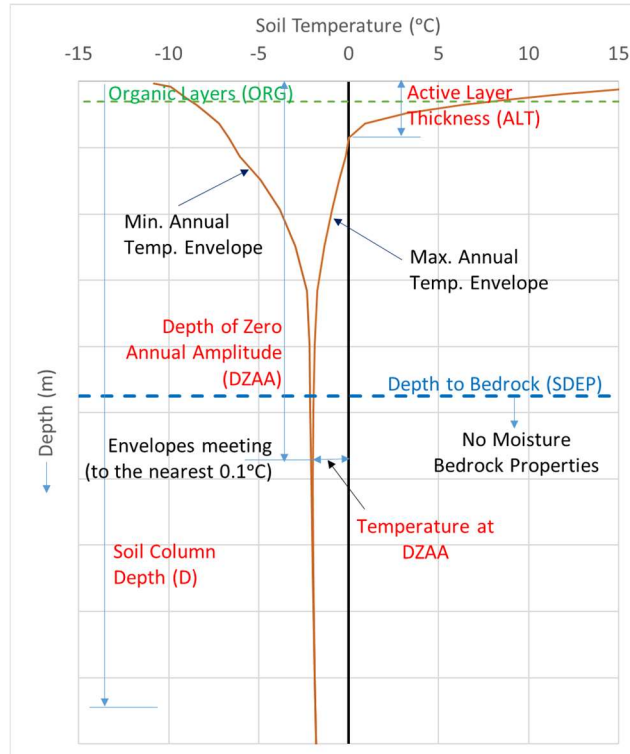
989 Zhang, T., Barry, R. G., Knowles, K., Heginbottom, J. A. and Brown, J.: Polar Geography Statistics and
990 characteristics of permafrost and ground-ice distribution in the Northern Hemisphere, ,
991 doi:10.1080/10889370802175895, 2008.

992 Zhang, X., Flato, G., Kirchmeier-Young, M., Vincent, L. A., Wan, H., Wang, X., Rong, R., Fyfe, J. C. and L, G.:
993 Changes in Temperature and Precipitation Across Canada, in Canada's Changing Climate Report, edited
994 by E. Bush and D. S. Lemmen, pp. 112–193, Ottawa, Ontario., 2019.

995 Zhang, Y., Cheng, G., Li, X., Han, X., Wang, L., Li, H., Chang, X. and Flerchinger, G. N.: Coupling of a
996 simultaneous heat and water model with a distributed hydrological model and evaluation of the combined
997 model in a cold region watershed, , doi:10.1002/hyp.9514, 2012.

998

Figures



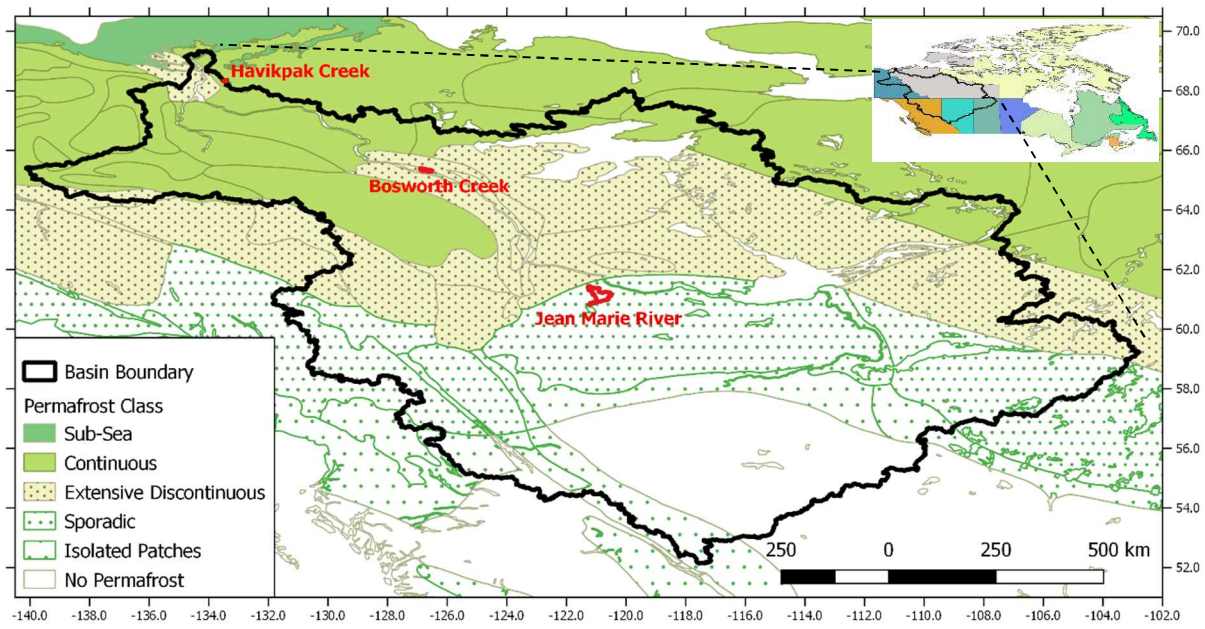
999

1000

Figure 1 Schematic of the soil column showing the variables used to diagnose permafrost

1001

1002

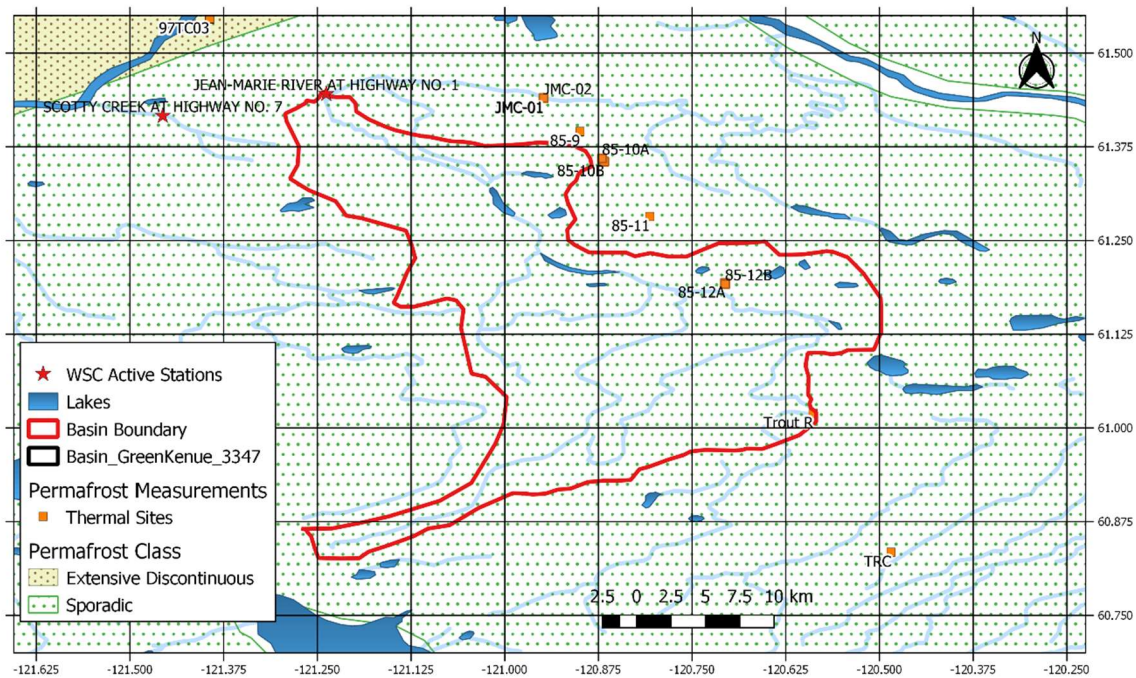


1003

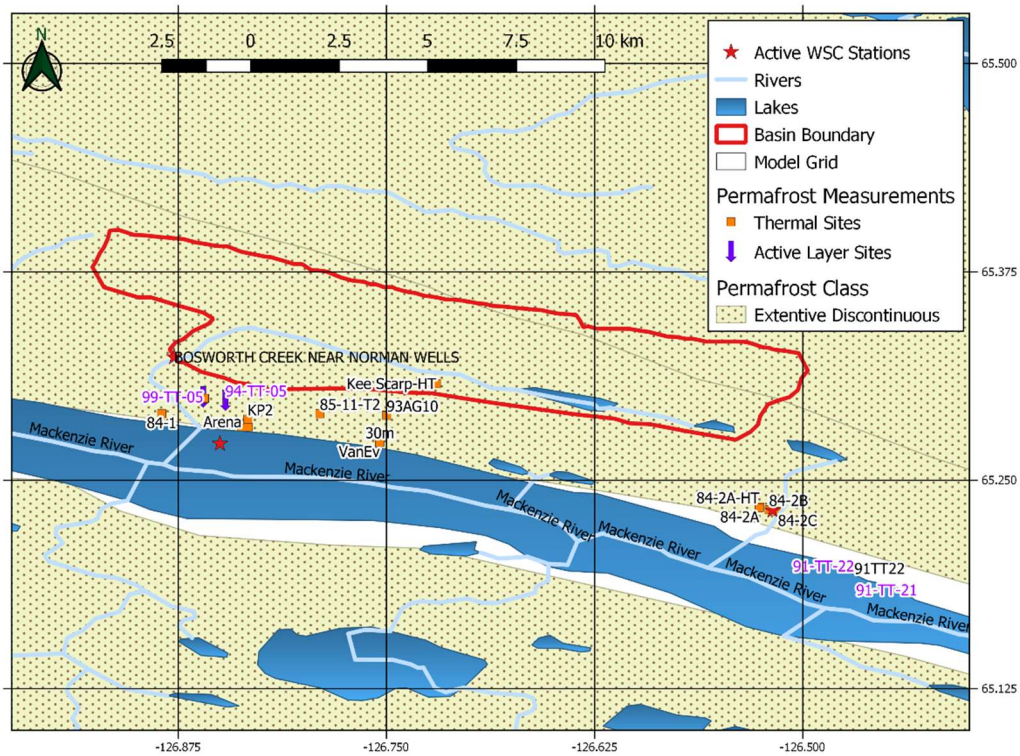
1004

Figure 2 Mackenzie River Basin: Location, permafrost classification, and the three study sites

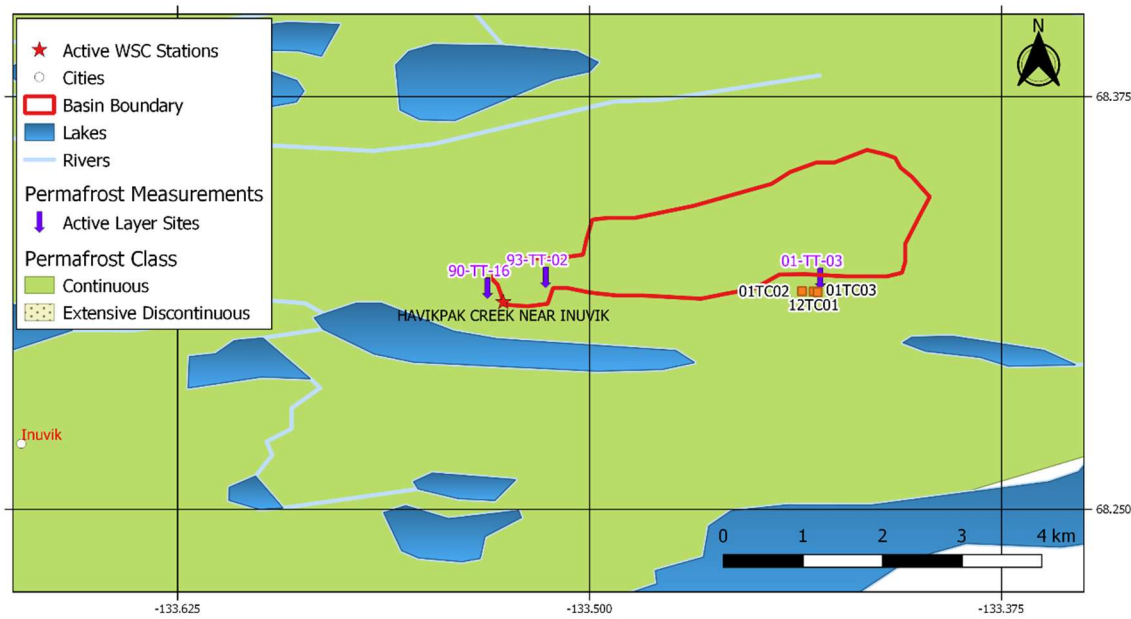
1005



a) Jean Marie River Basin



b) Bosworth Creek Basin

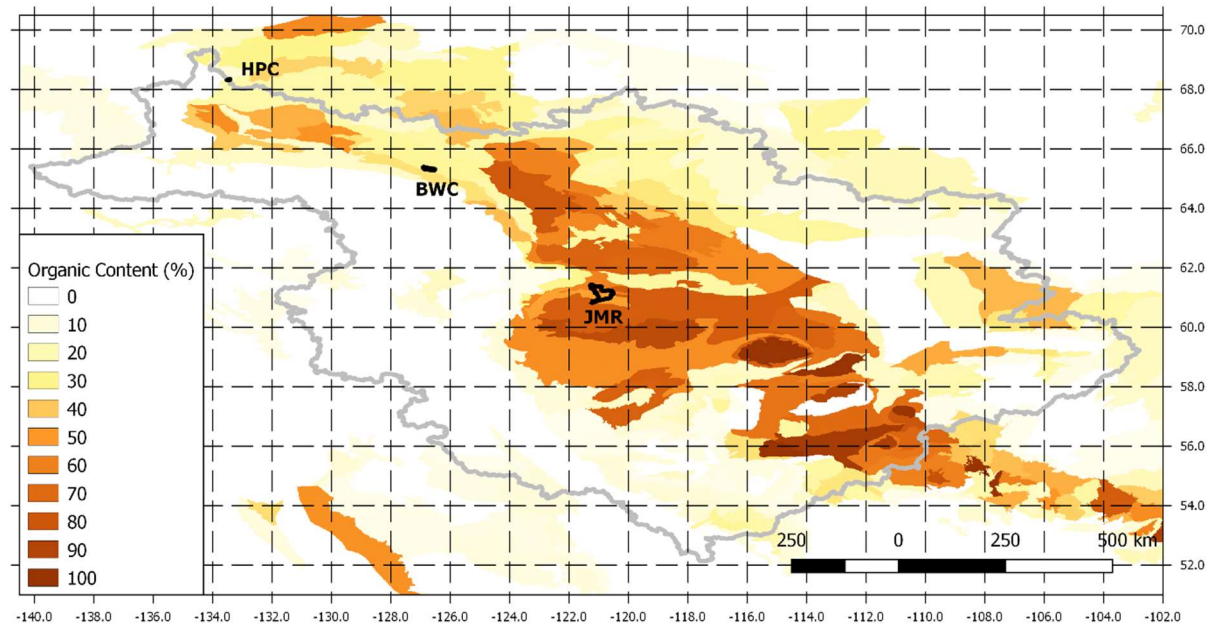


c) Havikpak Creek Basin

1006 *Figure 3 Location of and Permafrost measurement sites in a) Jean Marie River sub-basin, b) Bosworth*
 1007 *Creek sub-basin, and c) Havikpak Creek sub-basin*

1008

1009



1010

Figure 4 Gridded organic matter in soil at 0.125° resolution for the MRB, processed from the Soil Landscapes of Canada (SLC) v2.2 dataset (Centre for Land and Biological Resources Research, 1996)

1011

1012

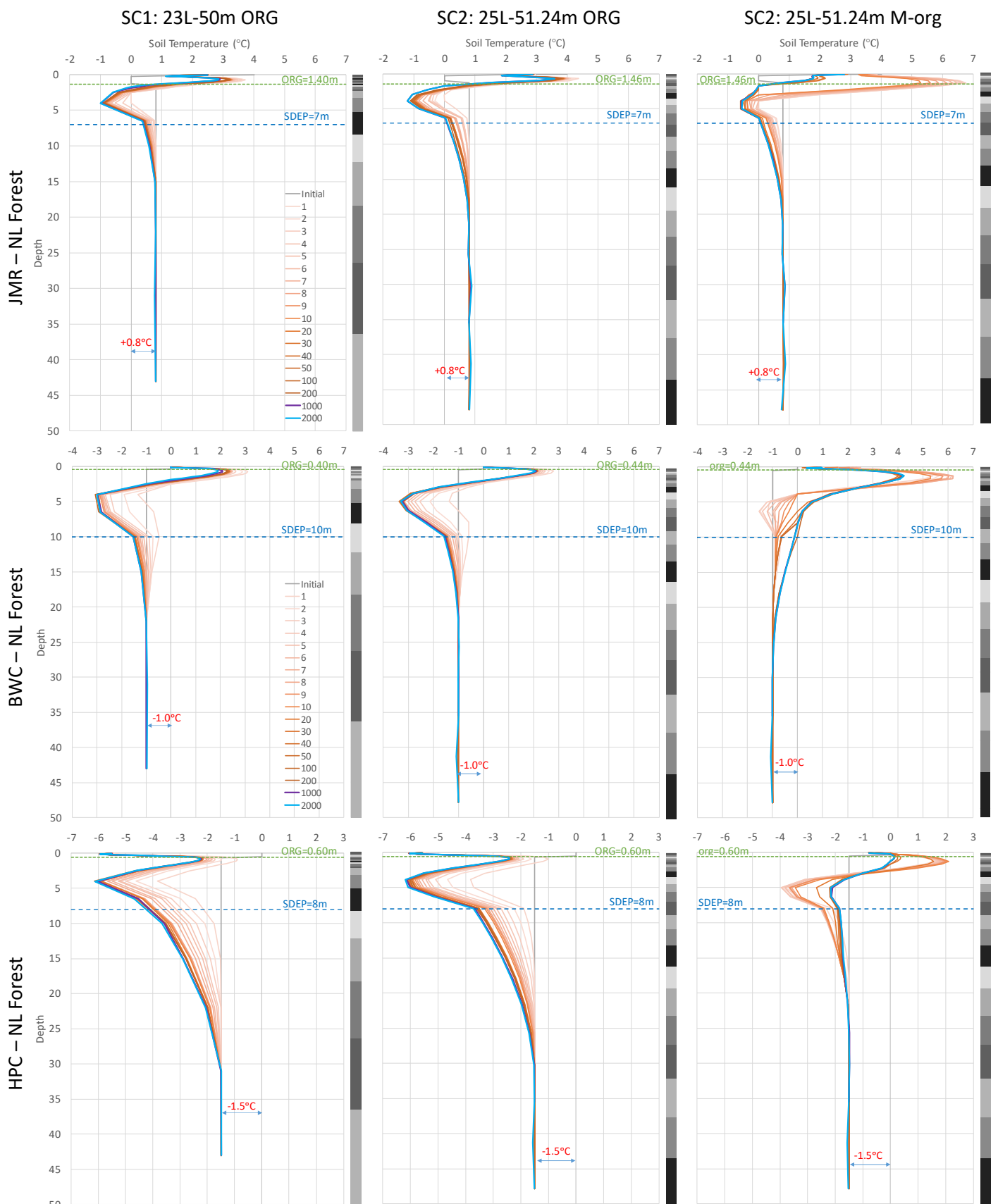


Figure 5 Soil temperature profiles at the end of selected spin-up Cycles for the NL Forest GRU at all three sites using different soil layering schemes and organic configurations

SC1: 23L-50m ORG

SC2: 25L-51.24m ORG

SC2: 25L-51.24m M-org

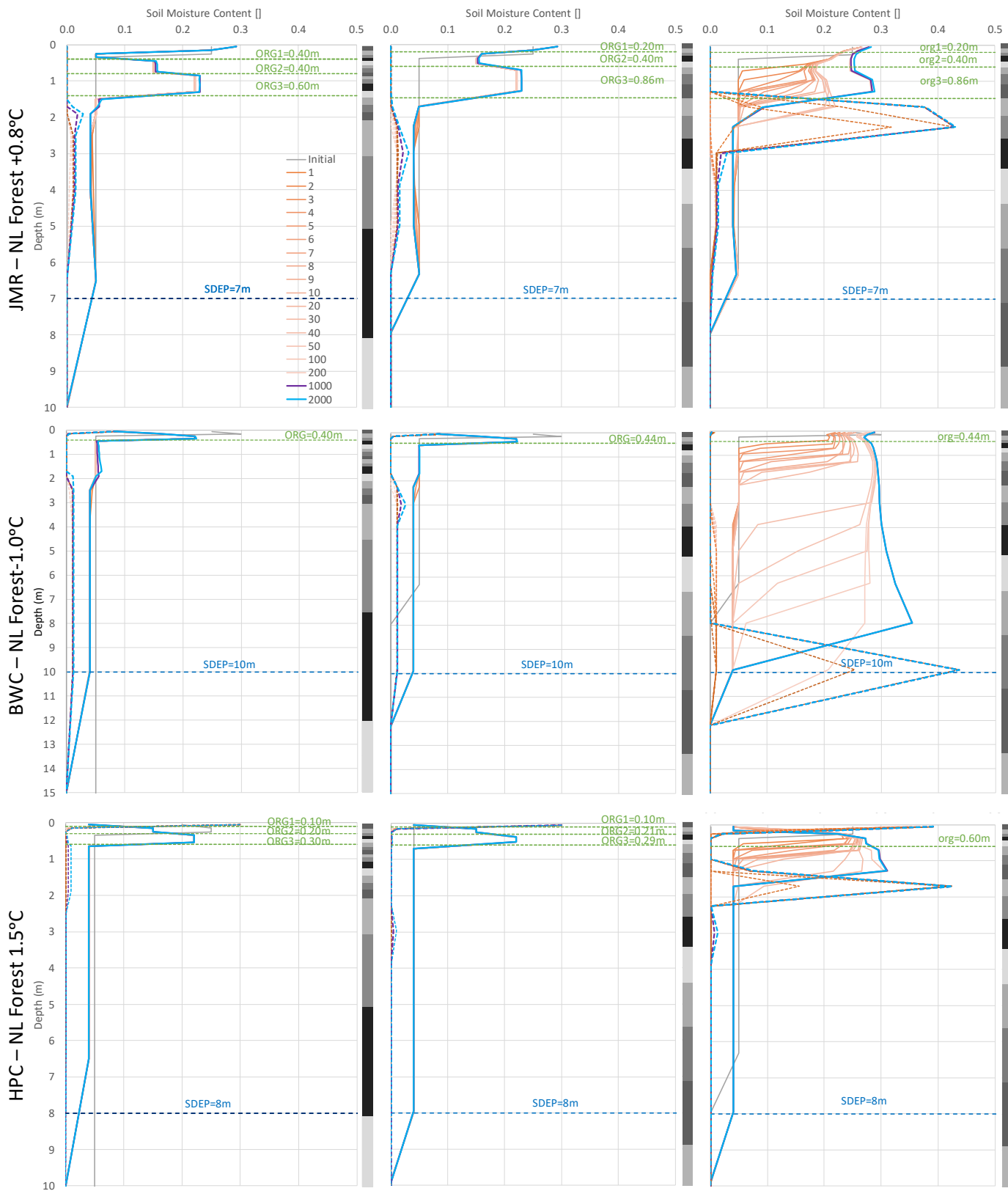
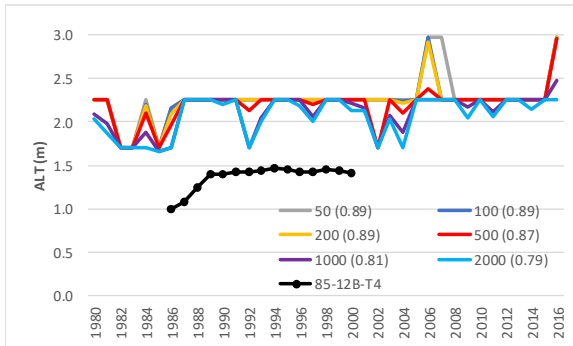


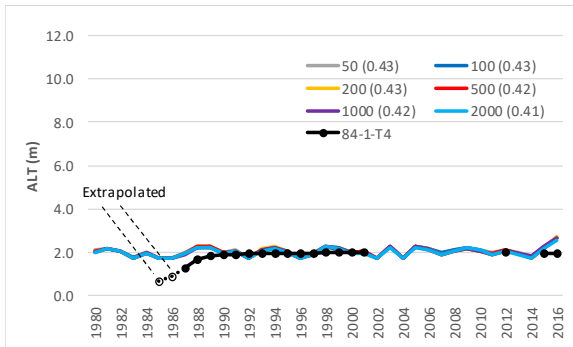
Figure 6 Soil moisture profiles at the end of selected spin-up cycles for the NL Forest GRU at all three sites using different soil layering schemes and organic configurations (solid lines for liquid and dashed lines for ice)



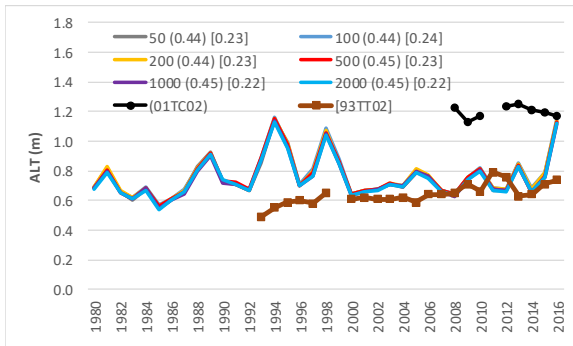
Figure 7 Impact of the soil layering scheme selection on spin-up convergence at the three study sites (the darker the color, the deeper the layer, deepest layer is colored blue)



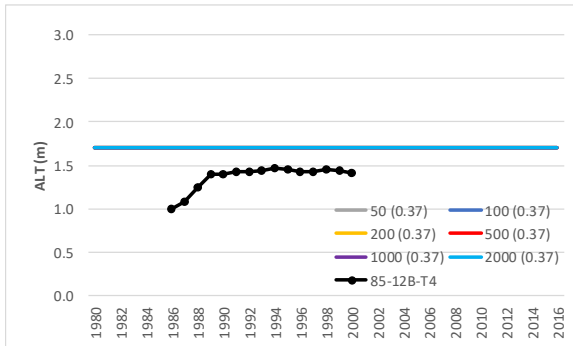
JMR – NL Forest (1.46m ORG +0.8°C SDEP7)



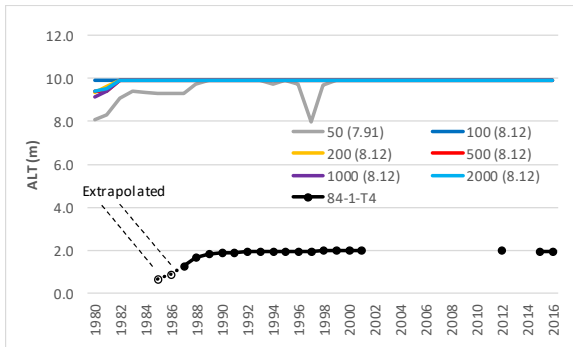
BWC – NL Forest (0.44m ORG -1.0°C SDEP10)



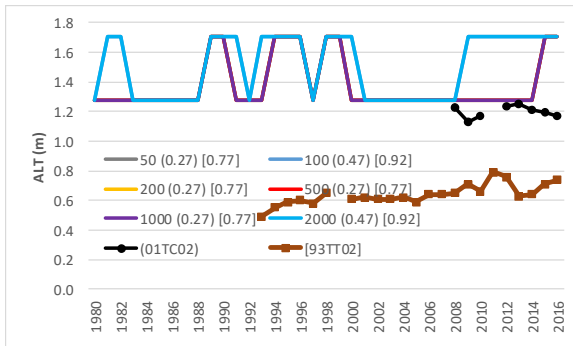
HPC – NL Forest (0.6m ORG -1.5°C SDEP8)



JMR – NL Forest (1.46m M-org +0.8°C SDEP7)

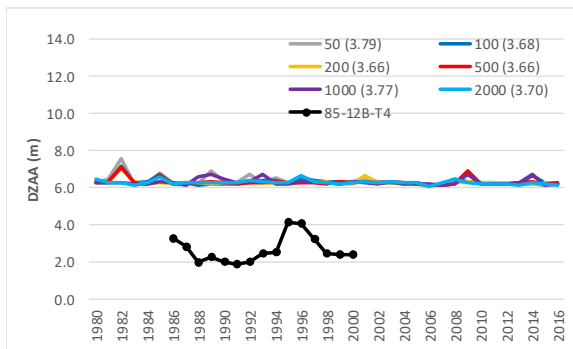


BWC – NL Forest (0.44m M-org -1.0°C SDEP10)

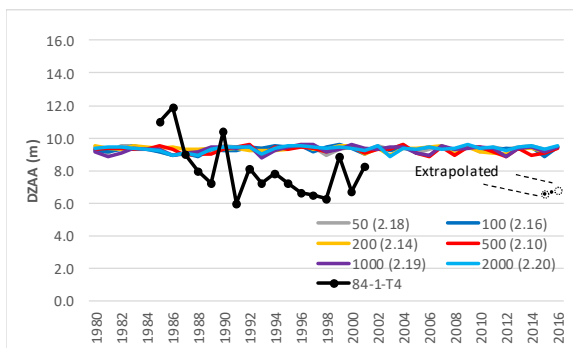


HPC – NL Forest (0.6m M-org -1.5°C SDEP8)

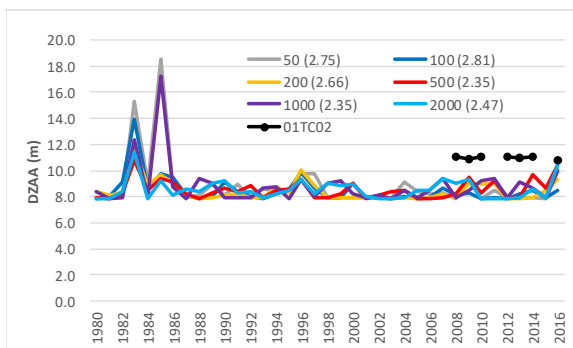
Figure 8 Impact of the number of spin-up cycles on simulated ALT on the Needleleaf Forest GRU at all sites – 2 organic configurations were used for each site using SC2 layering scheme, RMSE is shown in parenthesis



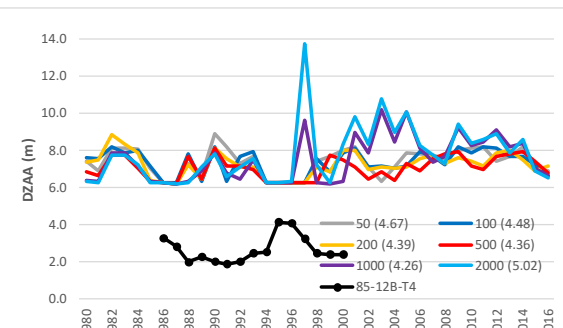
JMR – NL Forest (1.46m ORG +0.8°C SDEP7)



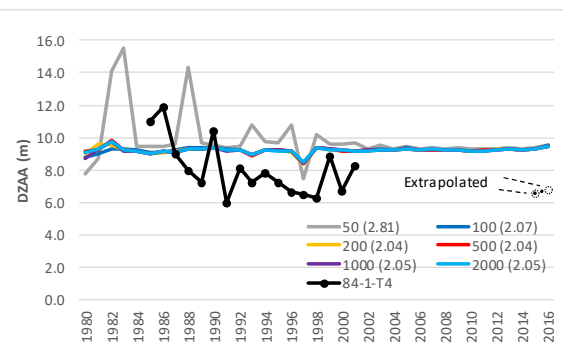
BWC – NL Forest (0.44m ORG -1.0°C SDEP10)



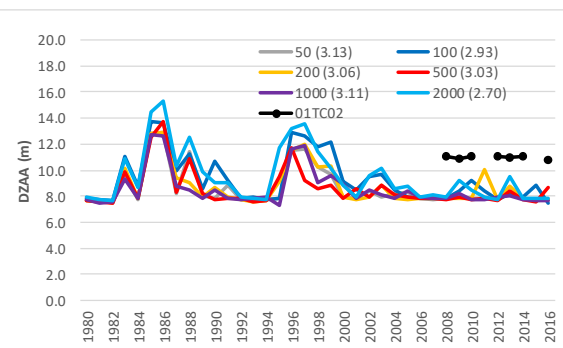
HPC – NL Forest (0.6m ORG -1.5°C SDEP8)



JMR – NL Forest (1.46m M-org +0.8°C SDEP7)



BWC – NL Forest (0.44m M-org -1.0°C SDEP10)



HPC – NL Forest (0.6m M-org -1.5°C SDEP8)

Figure 9 Impact of the number of spin-up cycles on simulated DZAA on the Needleleaf Forest GRU at all three sites – 2 organic configurations were used for each site using SC2 layering scheme, RMSE is shown in parenthesis

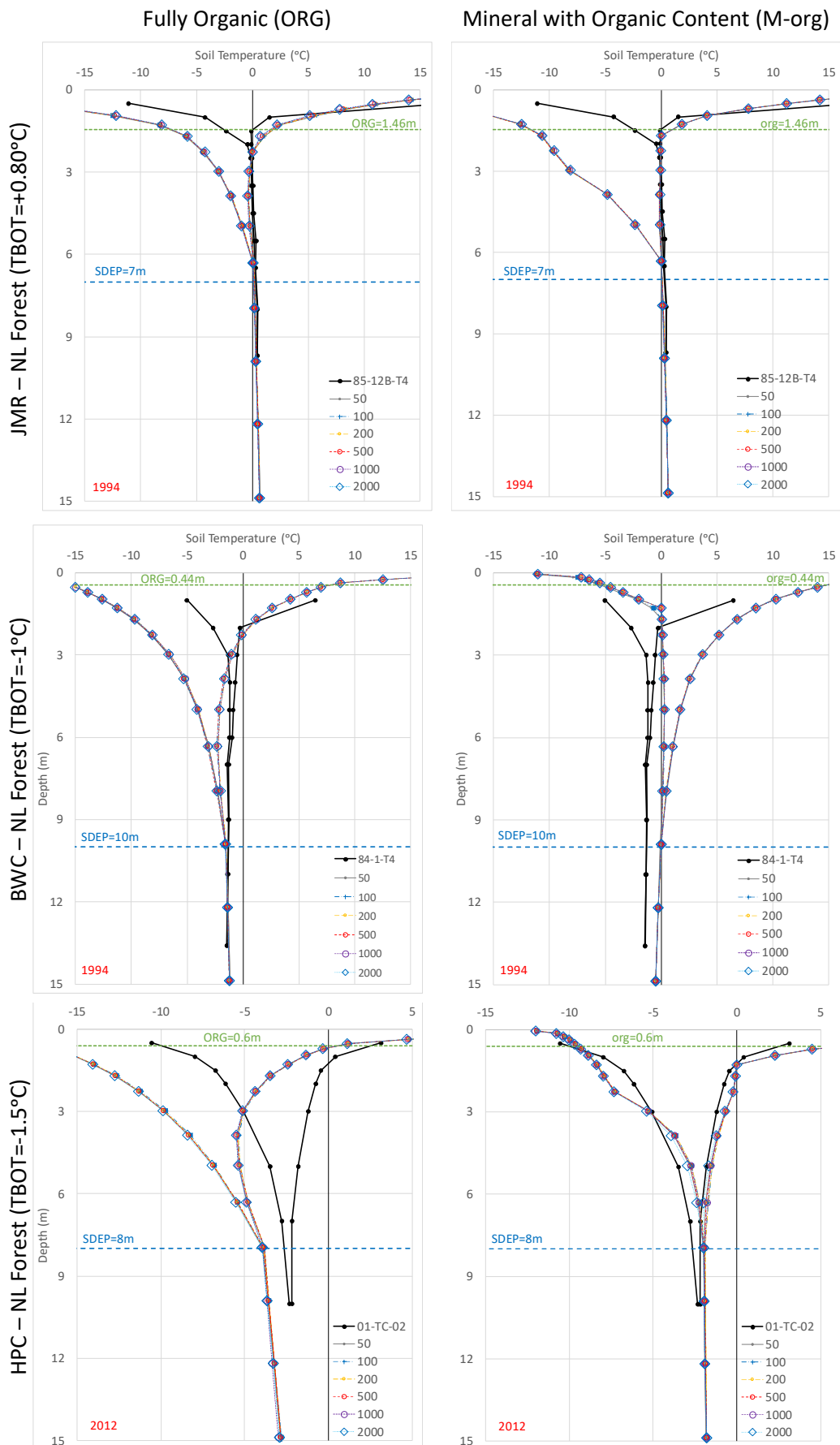


Figure 10 Impact of the number of spin-up cycles on simulated temperature envelopes for the Needleleaf Forest GRU for a selected year at each study site – 2 organic configurations used for each site using SC2 layering scheme

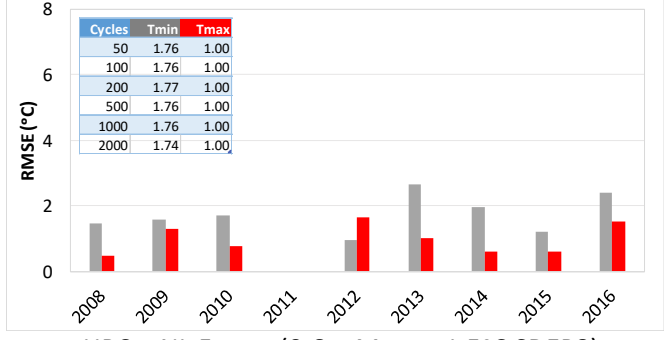
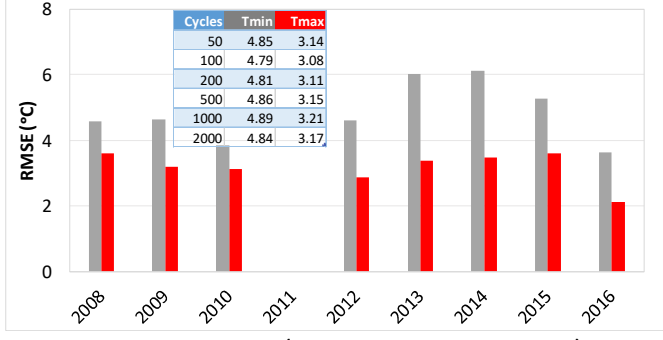
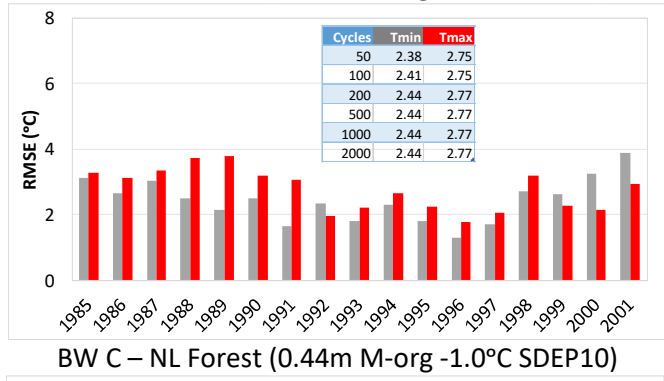
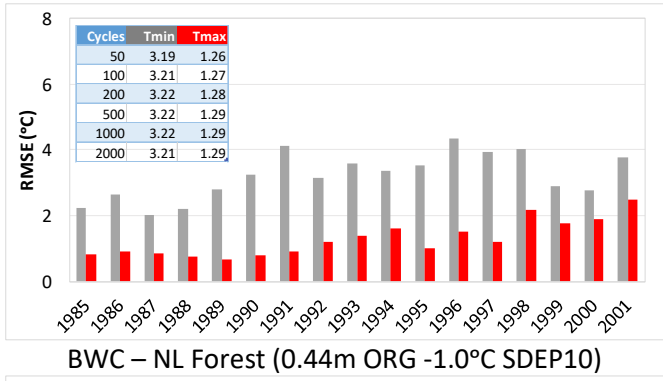
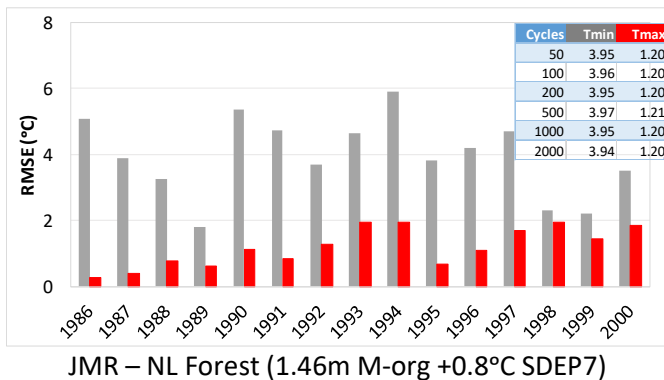
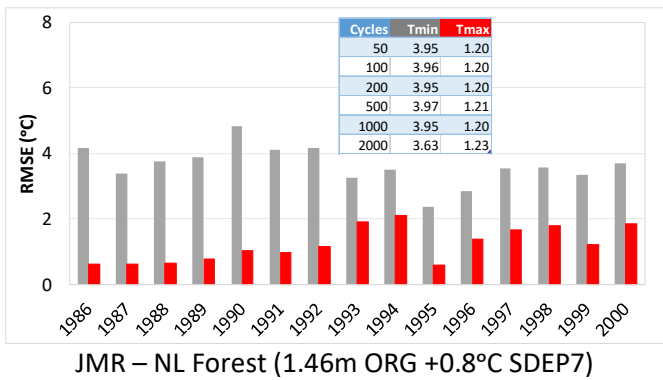


Figure 11 Time series of RMSE of simulated envelopes at all three sites at the end of 2000 cycles

2 organic configurations were used for each site using SC2 layering scheme

Table insets show the change in mean RMSE over the period of available record for simulations initiated after the shown number of spin-up cycles

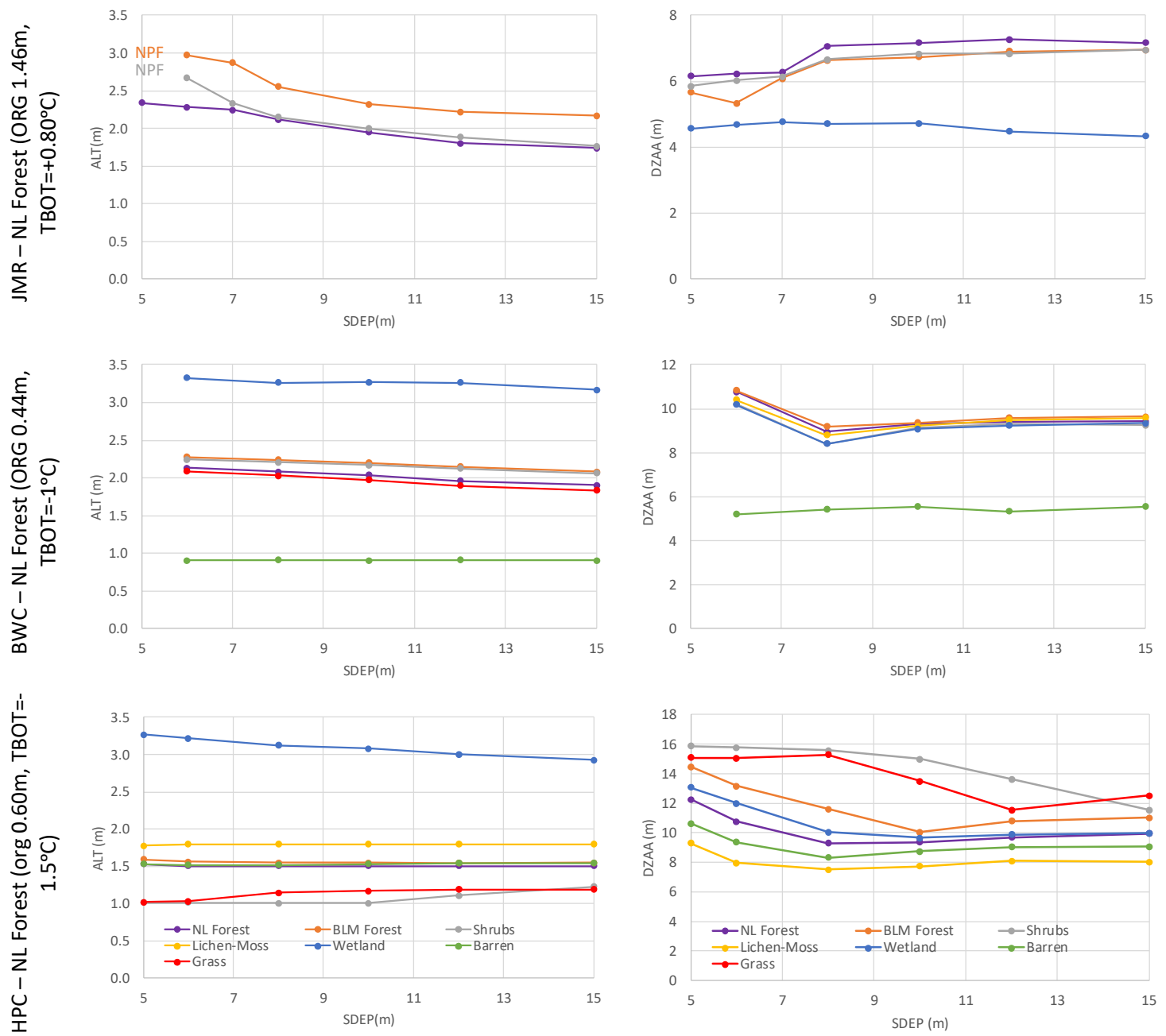


Figure 12 Impact of SDEP on average simulated ALT and DZAA for different GRUs at the three study sites over the 1980-2016 period

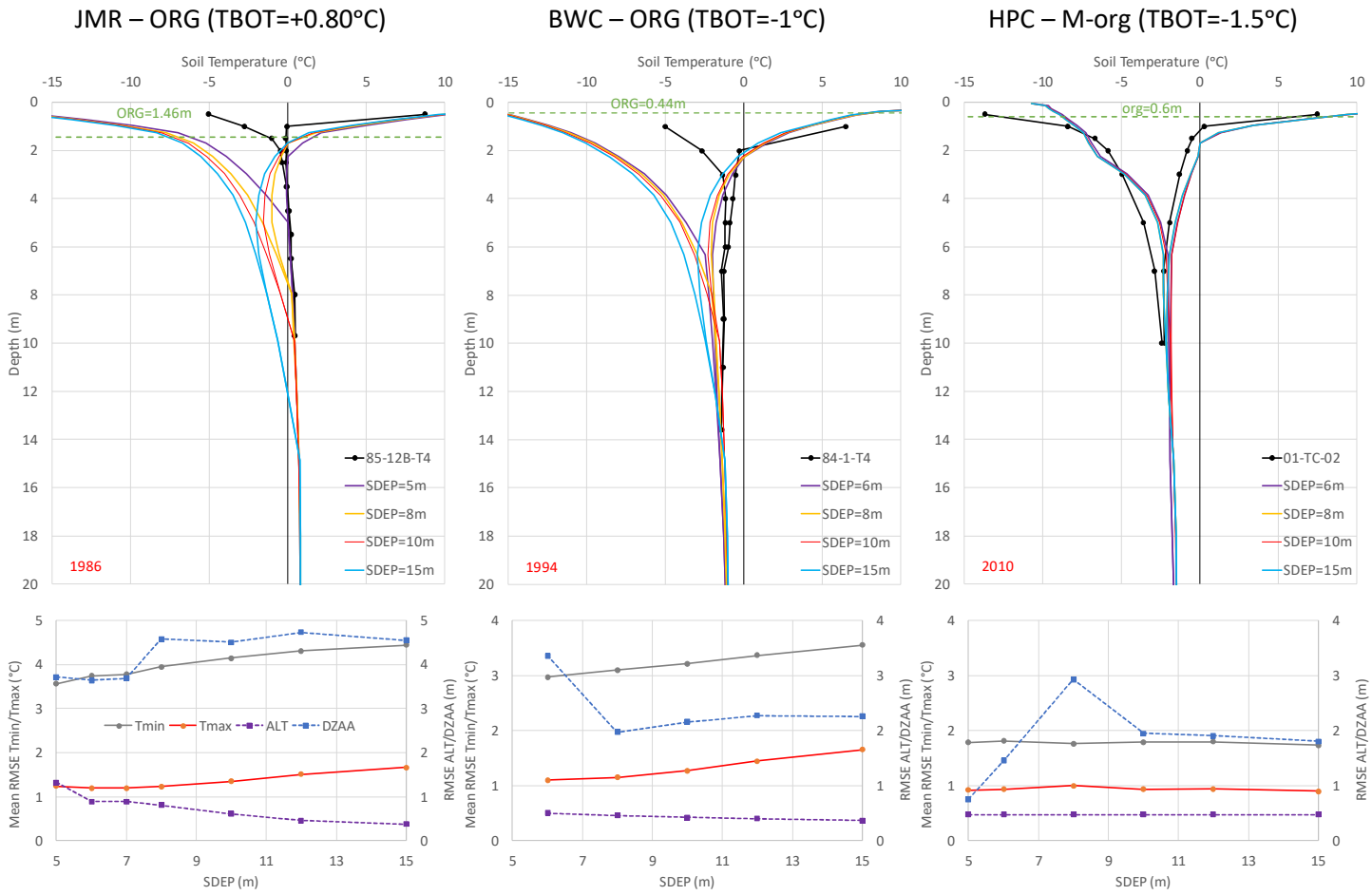


Figure 13 Impact of SDEP on simulated temperature envelopes for a selected year (top panel) and RSME for envelopes, ALT and DZAA over the simulation period for the Needleleaf Forest GRU at each study site

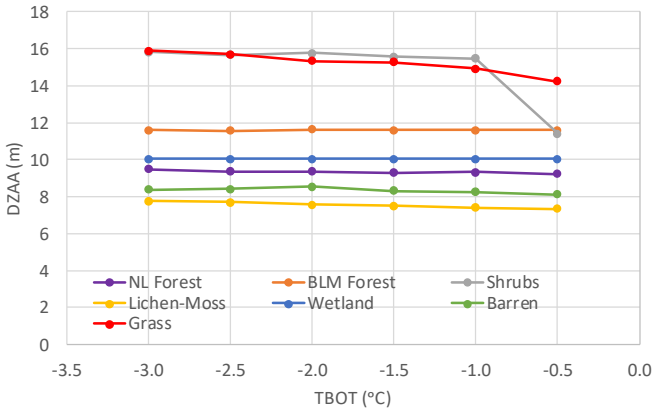
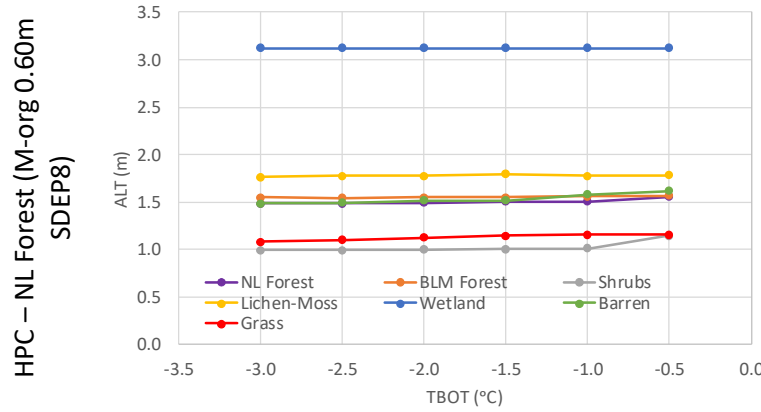
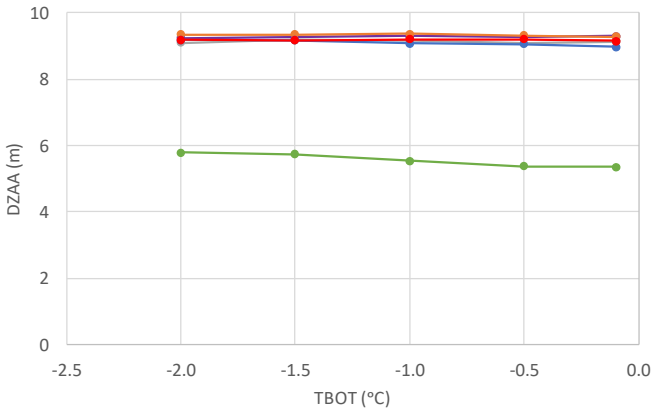
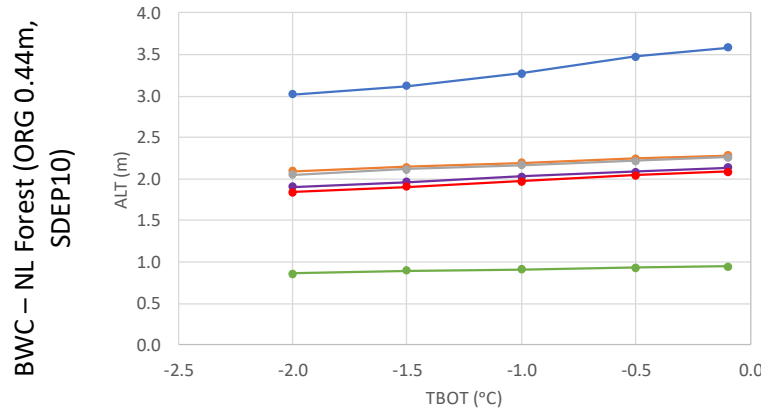
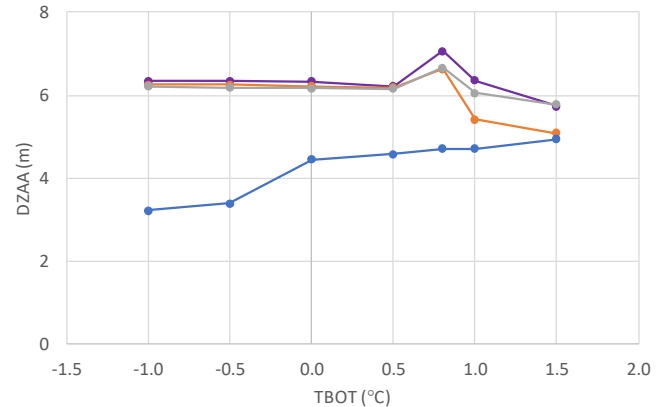
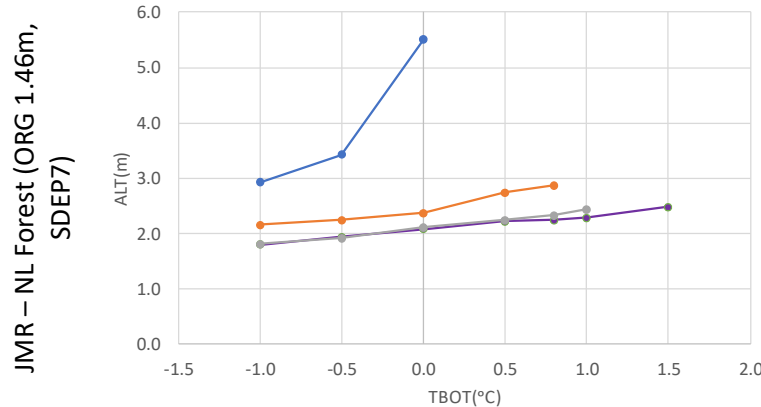
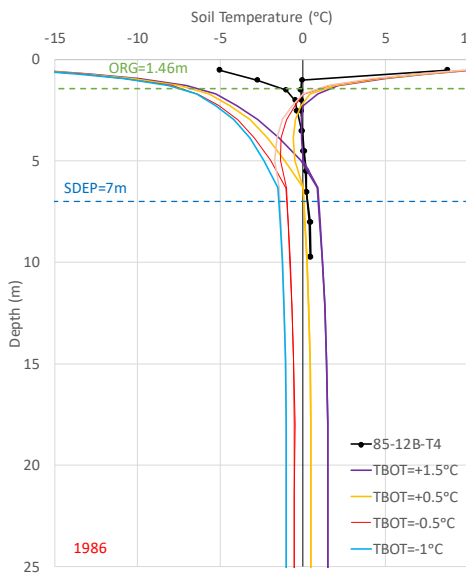
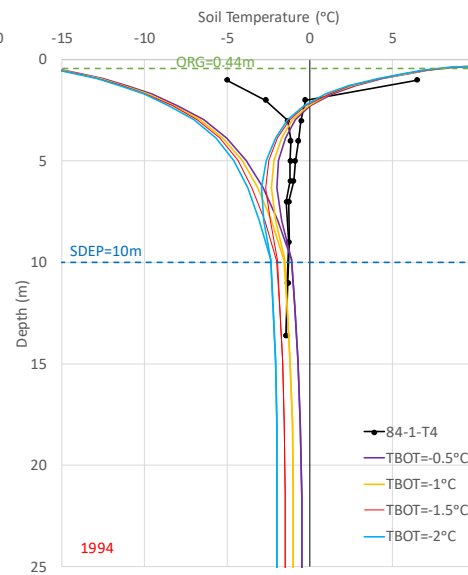


Figure 14 Impact of TBOT on average simulated ALT and DZAA for different GRUs at the three study sites over the 1980-2016 period

JMR – ORG



BWC – ORG



HPC – M-org

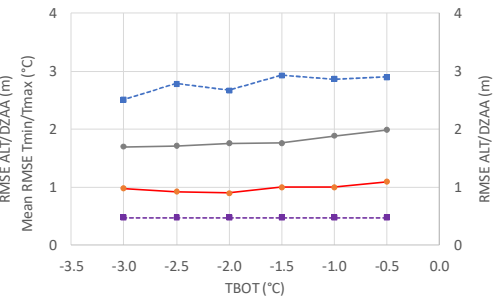
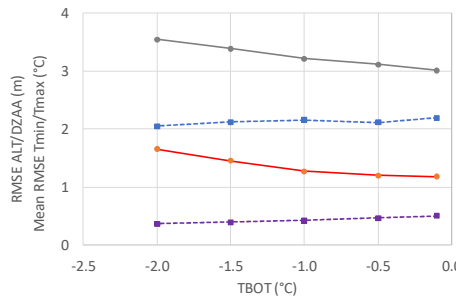
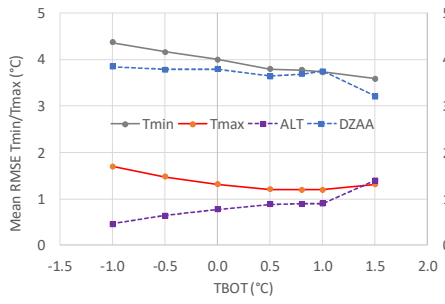
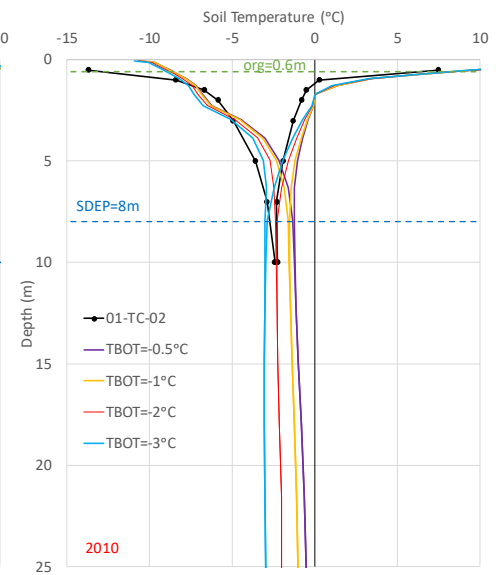


Figure 15 Impact of TBOT on simulated temperature envelopes for the Needleleaf Forest GRU for a selected year at each study site

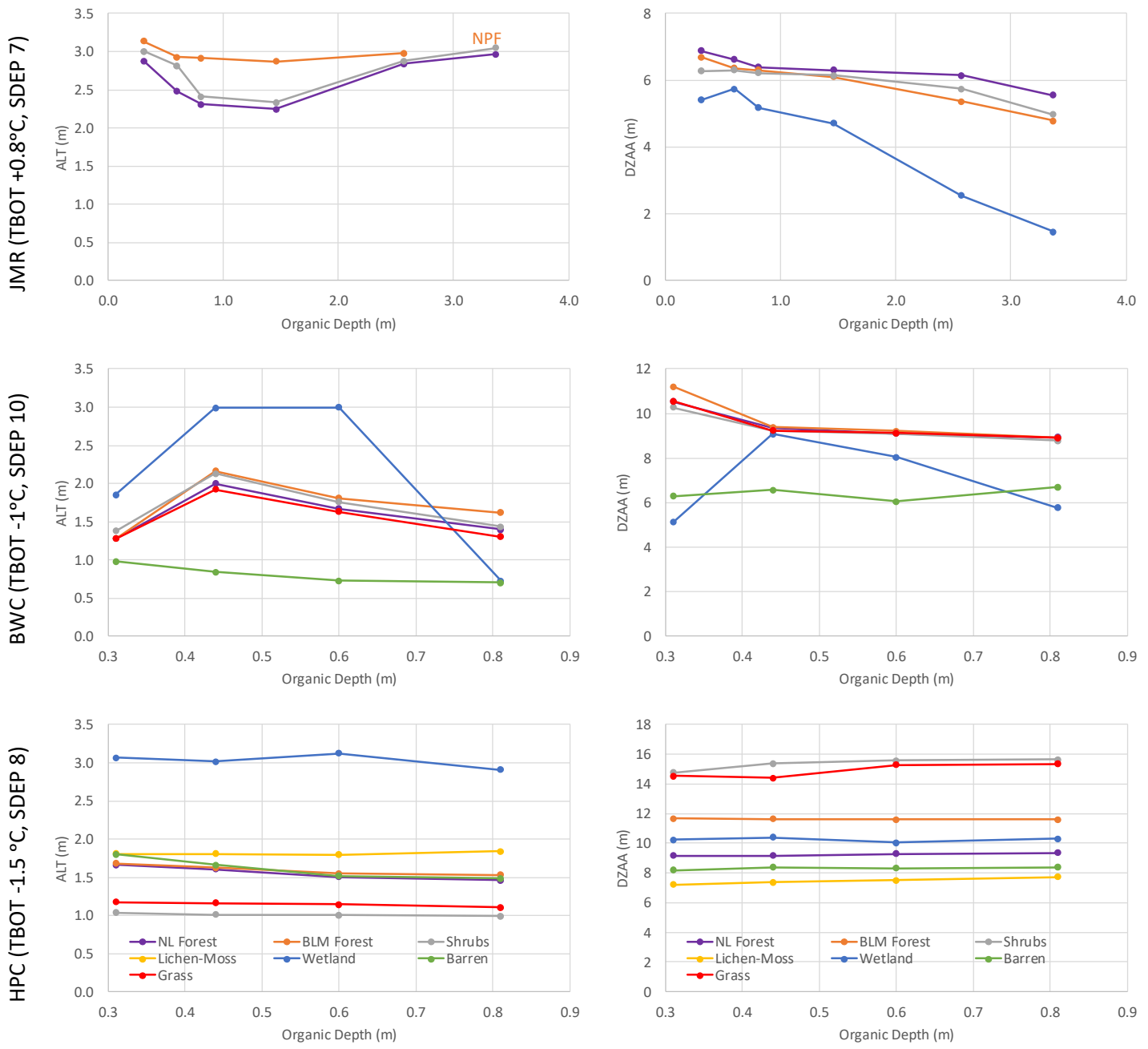


Figure 16 Impact of the depth of organic soil layers on average simulated ALT and DZAA for different GRUs at the three study sites for the 1980-2016 period

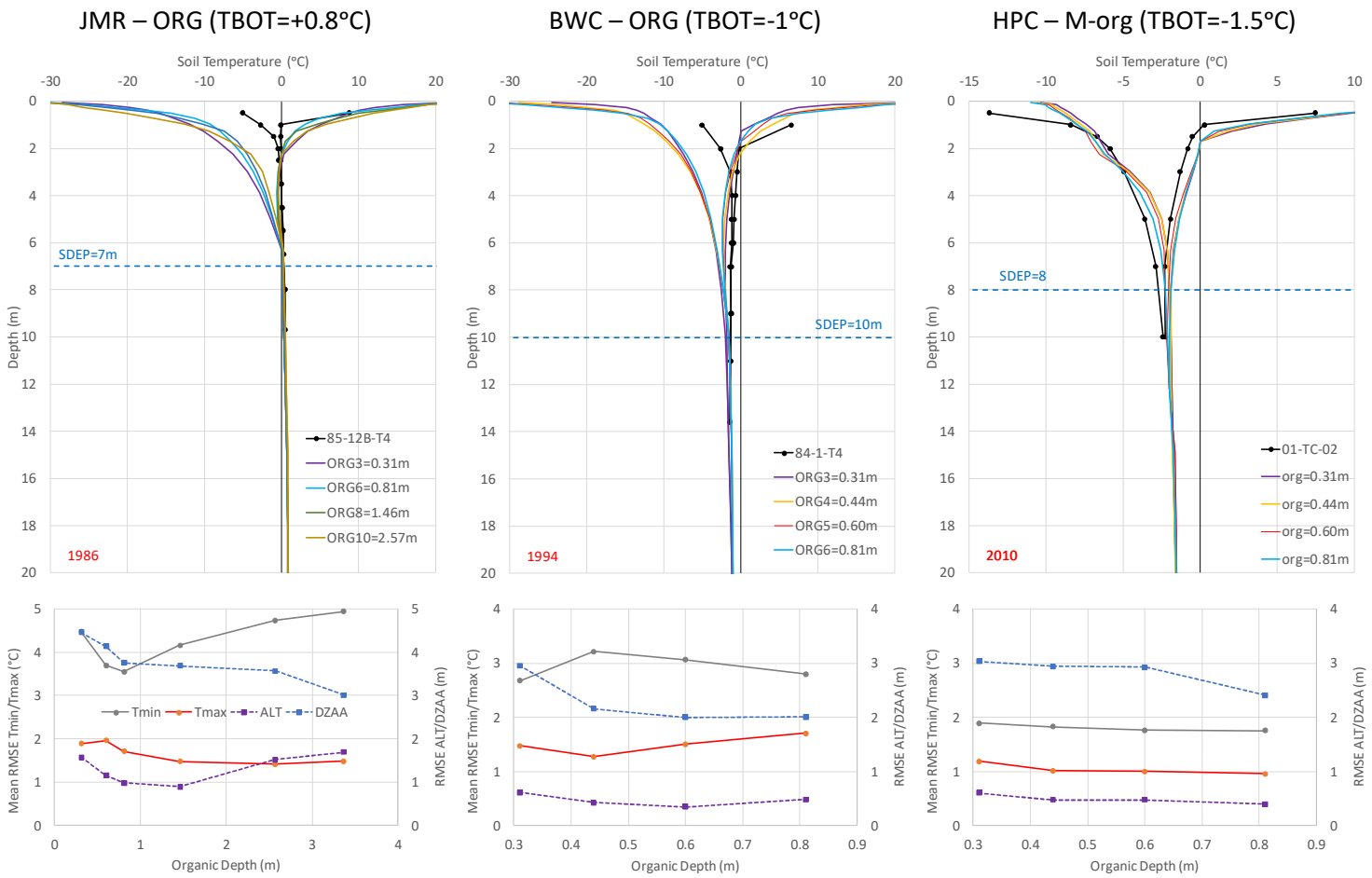


Figure 17 Impact of the depth of organic soil layers on simulated temperature envelopes for the Needleleaf Forest GRU for a selected year at each study site

Tables

Table 1 Permafrost sites and important measurements for the study sites

Site Name	Site ID	Type	Cables (Depth in m)	Data*	Vegetation	Permafrost Condition
JMR (Fort Simpson)						
Jean-Marie Creek	JMC-01	Thermal	T1 (5)	2008-2016	Shrub Fen	No
	JMC-02	Thermal	T1 (5)	2008-2016	Needle Leaf Forest	No
Pump Station 3	85-9 (NWZ9)	Thermal	T1 (5), T2 (5), T3 (20), T4 (20)	1986-1995, 2012-2016	Needle Leaf Forest/Shrubs/ Moss	No
Jean Marie Creek A	85-12A	Thermal	T1 (5), T2 (5), T3 (16.4), T4 (12)	1986-1995		No
Jean Marie Creek B	85-12B (NWZ12)	Thermal	T1 (5), T2 (5), T3 (17.2), T4 (9.7)	1986-2000		Yes
Mackenzie Hwy S	85-10A	Thermal	T1 (5), T2 (5), T3 (20), T4 (20)	1986-1995	N/A	No
	85-10B	Thermal	T1 (5), T2 (5), T3 (10.5), T4 (10.5)	1986-1995	N/A	No
Moraine South	85-11	Thermal	T1 (5), T2 (5), T3 (12), T4 (12)	1986-1995, 2014-2016	N/A	No
BWC (Norman Wells)						
NW Fen	99-TT-05	Thaw Tube		2009	Needle Leaf Forest/Moss	Yes
	99-TC-05	Thermal	Near Surface	2004-2008		
Normal Wells Town	Arena	Thermal	T1 (16)	2014-2015	Disturbed area adjacent to parking lot	Yes
	WTP	Thermal	T1 (30)	2014-2017		Yes
KP 2 - Off R.O.W.	94-TT-05	Thaw Tube		1995-2007	Needle Leaf Forest/Shrubs/ Moss	Yes
Norman Wells (Pump Stn 1)	84-1	Thermal	T1 (5.1), T2 (5), T3 (10.4), T4 (13.6), T5 (19.6)	1985-2000 1985-2016		Yes
van Everdingen	30m	Thermal	T1 (30)	2014-2017	Needle Leaf /Mixed Forest	Yes
Kee Scrap	Kee Scrap-HT	Thermal	T1 (128)	2015-2017	Mixed Forest	No
HPC (Inuvik)						
Havikpak Creek	01-TT-02	Thaw Tube		1993-2017	Needle Leaf Forest	Yes
Inuvik Airport	01-TT-03	Thaw Tube		2008-2017		Yes
Inuvik Airport	90-TT-16	Thaw Tube		2008		Yes
Upper Air	01-TT-02	Thaw Tube		2008-2017	N/A	Yes
Inuvik Airport (Trees)	01-TC-02	Thermal	T1 (10)	2008-2017	Needle Leaf Forest	Yes
Inuvik Airport (Bog)	01-TC-03	Thermal	T1 (8.35)		Wetland	Yes
	12-TC-01	Thermal	T1 (6.5)	2013-2017		Yes

Table 2 Soil profile layering schemes

Layer	First Scheme (SC1)			Second Scheme (SC2)		
	Thickness	Bottom	Center	Thickness	Bottom	Center
1	0.10	0.10	0.05	0.10	0.10	0.05
2	0.10	0.20	0.15	0.10	0.20	0.15
3	0.10	0.30	0.25	0.11	0.31	0.26
4	0.10	0.40	0.35	0.13	0.44	0.38
5	0.10	0.50	0.45	0.16	0.60	0.52
6	0.10	0.60	0.55	0.21	0.81	0.71
7	0.10	0.70	0.65	0.28	1.09	0.95
8	0.10	0.80	0.75	0.37	1.46	1.28
9	0.10	0.90	0.85	0.48	1.94	1.70
10	0.10	1.00	0.95	0.63	2.57	2.26
11	0.20	1.20	1.10	0.80	3.37	2.97
12	0.20	1.40	1.30	0.99	4.36	3.87
13	0.20	1.60	1.50	1.22	5.58	4.97
14	0.20	1.80	1.70	1.48	7.06	6.32
15	0.20	2.00	1.90	1.78	8.84	7.95
16	1.00	3.00	2.50	2.11	10.95	9.90
17	2.00	5.00	4.00	2.48	13.43	12.19
18	3.00	8.00	6.50	2.88	16.31	14.87
19	4.00	12.00	10.00	3.33	19.64	17.98
20	6.00	18.00	15.00	3.81	23.45	21.55
21	8.00	26.00	22.00	4.34	27.79	25.62
22	10.00	36.00	31.00	4.90	32.69	30.24
23	14.00	50.00	43.00	5.51	38.20	35.45
24				6.17	44.37	41.29
25				6.87	51.24	47.81

Table 3 The number of layers of each organic sub-type for fully organic soil configurations (ORG) and organic content for mineral configurations (M-org)

# Organic layers	Organic Sub-Type (ORG)			Organic Content % (M-org)		
	1 (Fibric)	2 (Hemic)	3 (Sapric)	JMR	BWC	HPC
3	1	1	1			3@18, 0 →
4	1	1	2		2@35, 30, 25, 0 →	4@18, 0 →
5	1	2	2			4@18, 0 →
6	2	2	2			4@18, 0 →
8*	2	3	3	2@60, 2@50, 2@40, 30 →		
10*	3	3	4			
11*	3	4	4			

*Only used for JMR, x@y means x layers with the specified %, and x → means the value is for the remainder of the layers below

Table 4 Comparison of temperature and precipitation of the selected spinning year to mean climate of the WFDEI Dataset

Site	Mean Annual Temperature (°C)			Total Annual Precipitation (mm/yr)		
	WFDEI 1979-2016		Oct 1979 – Sep 1980	WFDEI 1979-2016		Oct 1979 – Sep 1980
	Mean	Std Dev		Mean	Std Dev	
JMR	-2.65	1.06	-1.81	418.1	64.5	338.4
BWC	-5.65	1.01	-4.36	403.9	74.7	394.3
HPC	-8.73	1.17	-7.82	295.7	40.0	301.2